

1 Article

2

Anatomy, Age and Origin of an Intramontane Top

3

Basin Surface (Sorbas Basin, Betic Cordillera, SE

4

Spain)

5 **Martin Stokes** ^{1,*}, **Anne E. Mather** ¹, **Ángel Rodés** ², **Samantha H. Kearsey (née Ilott)** ¹,
6 and **Shaun Lewin** ¹7 ¹ School of Geography, Earth and Environmental Sciences, University of Plymouth, Drake Circus, Plymouth,
8 Devon, PL4 8AA, UK;9 ² NERC Cosmogenic Isotope Analysis Facility, Scottish Universities Environmental Research Centre,
10 Rankine Avenue, Scottish Enterprise Technology Park, East Kilbride, G75 0QF, UK;12 * Correspondence: mstokes@plymouth.ac.uk; Tel.: +44-1752-584772

13

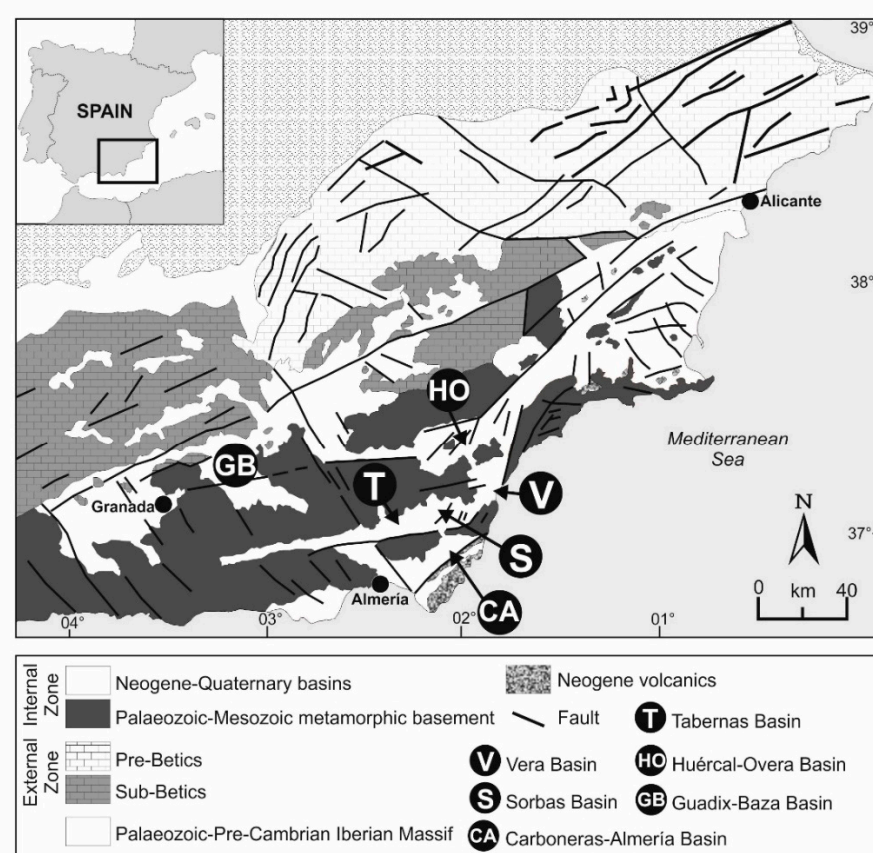
14 **Abstract:** Collisional mountain belts commonly develop intramontane basins from mechanical and
15 isostatic subsidence during orogenic development. These frequently display a relict top surface,
16 evidencing a change interval from basin infilling to erosion often via capture or overspill. Such
17 surfaces provide markers that inform on orogenic growth patterns via climate and base level
18 interplay. Here, we describe the top surface from the Sorbas Basin, a key intramontane basin within
19 the Betic Cordillera (SE Spain). The surface is fragmentary comprising high elevation hilltops and
20 discontinuous ridges developed onto the variably deformed final basin infill outcrop (Gochar
21 Formation). We reconstruct surface configuration using DEM interpolation and apply ¹⁰Be/²⁶Al
22 cosmonuclides to assess surface formation timing. The surface is a degraded Early Pleistocene
23 erosional pediment developed via autogenic switching of alluvial fan streams under stable dryland
24 climate and base level conditions. Base level lowering since the Middle Pleistocene focused
25 headwards incision up interfan drainages, culminating in fan head capture and fan morphological
26 preservation within the abandoned surface. Post abandonment erosion has lowered the basin
27 surface by 31 m (average) and removed ~5.95 km³ of fill. Regional basin comparisons reveal a phase
28 of Early Pleistocene surface formation, marking landscape stability following the most recent
29 Pliocene-Early Pleistocene mountain building. Post-surface erosion rate quantification is low and in
30 accordance with ¹⁰Be denudation rates typical of the low uplift Betic Cordillera.31 **Keywords:** Intramontane basin; pediment; glaci; alluvial fan; river terrace; DEM; interpolation;
32 cosmonuclide, base level34

1. Introduction

35 Intramontane basins are areas of fault and fold-related subsidence that develop within an
36 evolving collisional mountain belt [1]. The tectonically dynamic nature of such settings means that
37 intramontane basins can cyclically form, fill and erode over geological timescales [2, 3]. The basins
38 can be internally drained, dominated by alluvial fan and lacustrine settings, but can then switch to
39 externally drained systems via lake overspill or river capture processes [4, 5]. Studies of intramontane
40 basins are either 1) geological, focussing on the sedimentary infill record for stratigraphic,
41 palaeoenvironmental and tectonic purposes [6] or 2) geomorphological, using inset river-fan-lake
42 terrace levels to reconstruct the basin incisional history linked to tectonic-climatic-capture-related
43 changes in sediment supply and base level [7]. A key, but often overlooked stratigraphic unit is the
44 surface that caps the final stage of intramontane basin infill. This surface can be 1) depositional, with
45 a morphology reflecting the final depositional environment(s) (alluvial fan / lake) or 2) erosional,

46 formed by regional subaerial processes. Such 'epigene' land surfaces (*sensu* [8]) are scientifically
 47 important because they mark the point at which the basin has switched from erosion to deposition
 48 [9]. Furthermore, they can act as a regional marker, providing insight into patterns and drivers of the
 49 onset and subsequent basin incision [10] or as a marker for surface deformation assessments [11].
 50 However, these surfaces can be problematic to study due to poor preservation, post depositional
 51 modification and dating challenges meaning the surfaces often only attract peripheral attention as
 52 the respective end or start points of geological and geomorphological research. For example, surface
 53 remnants are often highly fragmentary and can be degraded by erosion or deformation causing
 54 across basin or between basin correlation problems [12, 13]. Once abandoned, the surface can become
 55 modified due to cementation by pedogenic or groundwater processes [14]. Surface dating can be a
 56 significant challenge due to technique limitations or material suitability issues collectively related to
 57 surface composition, degradation because of surface antiquity (i.e. surface is beyond the technique
 58 age range limit) and post depositional degradation and modification also linked to antiquity [15,16].
 59 To explore and overcome some of these challenges and to highlight the importance of intramontane
 60 top basin surfaces for understanding sedimentary basin evolution and longer-term Quaternary
 61 landscape development we examine the Sorbas Basin in SE Spain (Figure 1). The Sorbas Basin is a
 62 medium sized (30x20 km) Neogene sedimentary basin that has developed as part of the ongoing fault
 63 and fold related uplift of the Betic Cordillera, a major Alpine mountain range, formed because of the
 64 ongoing Africa-Europe collision [1]. The basin fill is dominated by marine Miocene sedimentation
 65 [17,18], with continental sedimentation forming the final stages of basin infill (Gochar Formation
 66 [19,20]).

67



68

69 **Figure 1.** Tectonic zonation of the Betic Cordillera and key intramontane basins referred to within the
 70 text (modified from [21-23]).

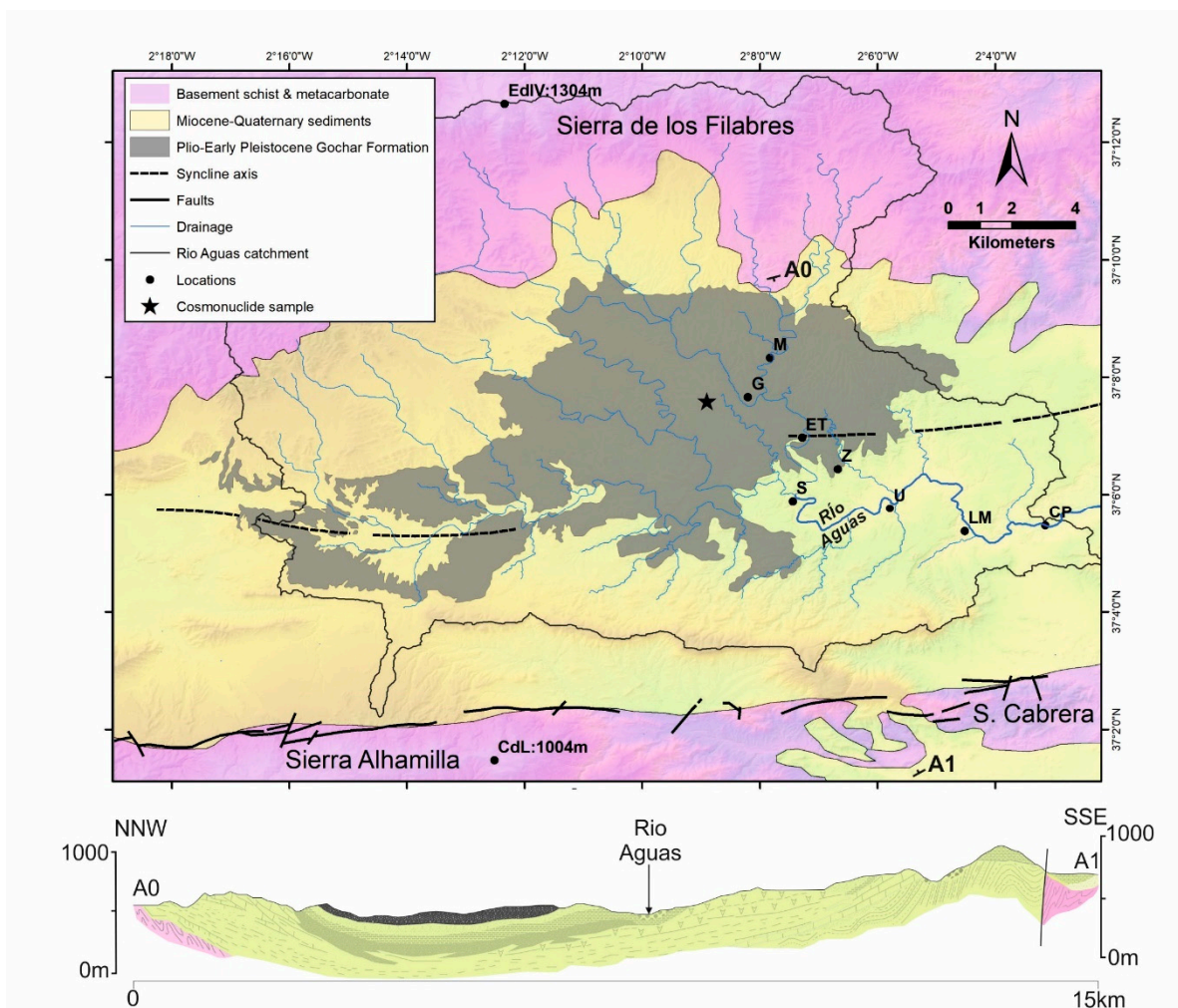
71

72 A surface is developed onto the final stage of basin fill, commonly referred to as the "Gochar
 73 Surface" by studies examining long-term drainage evolution [10, 25]. The purpose of this paper is to:
 74 1) describe the relict morphology of the basin surface, 2) to digitally reconstruct the surface using

75 interpolation of surface remnants, 3) to provide age estimates for surface development using
 76 cosmonuclide dating; 4) to use the interpolated and dated surface to quantify spatial and temporal
 77 patterns of basin erosion and 5) to consider the development of the surface as a Quaternary landscape
 78 feature in the context of the ongoing cyclic development of an intramontane basin.
 79

80 2. Geological and Geomorphological Background

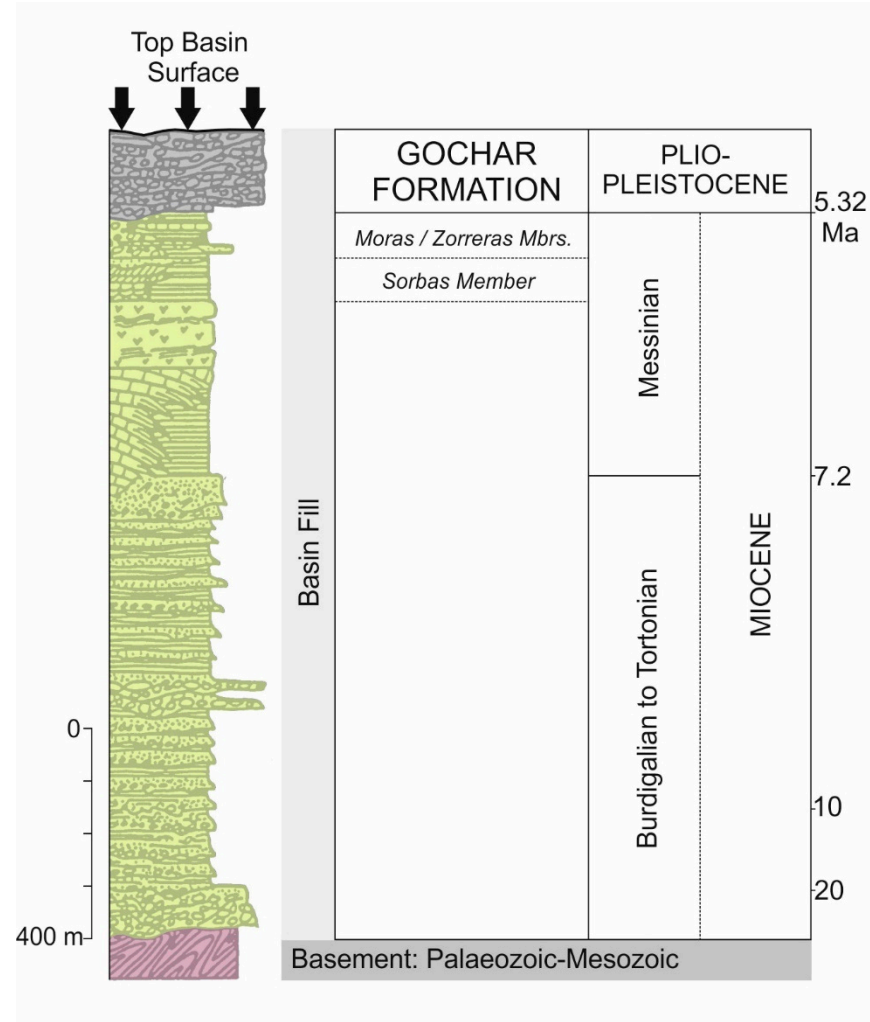
81 The Sorbas Basin (Figures 1 and 2) is one of a series of Neogene intramontane sedimentary basins
 82 within the Betic Cordillera [2]. It is defined to the north and south by mountain ranges of



83
 84 **Figure 2.** Simplified Sorbas Basin geology map and cross section [modified from [19, 25, 26]]. EdIV =
 85 Ermita de la Virgen; M = Moras; G = Gochar; ET = El Tieso; S = Sorbas, Z = Zorreras; U = Urra; LM =
 86 Los Molinos; CP = capture point; CdL = Cerron de Lucainena; A0-A1 = line of section.

87 metamorphic basement (Figure 2) that are organized into km-scale regional antiformal fold structures
 88 formed in consequence of Miocene-Recent collision-related tectonic denudation [27, 28]. The Sierra
 89 de los Filabres to north peaks at 1304 m (Ermita de la Virgen de la Cabeza) and comprises an embayed
 90 non-faulted mountain front with a relief of up to 700 m. To the south, the Sierra Alhamilla is
 91 characterised by a linear faulted mountain front [29], peaking at 1004 m (Cerrón de Lucainena) and
 92 with a relief of ~400 m. The intervening basin is infilled with a sequence of Miocene to Quaternary
 93 marine and continental sediments that are folded into an open E-W orientated syncline structure
 94 (Figure 2). The basin narrows to the west and east, joining the adjacent Tabernas and Vera Basins,
 95 delimited by poorly defined topographic highs developed into the sedimentary infill.

96 Miocene marine sediments dominate the Sorbas Basin sedimentary infill (Figure 3), becoming
 97 progressively continental during the late Miocene represented by coastal plain sediments (Zorreras
 98 Member) and basin margin alluvial fan sequences (Moras Member) [19].



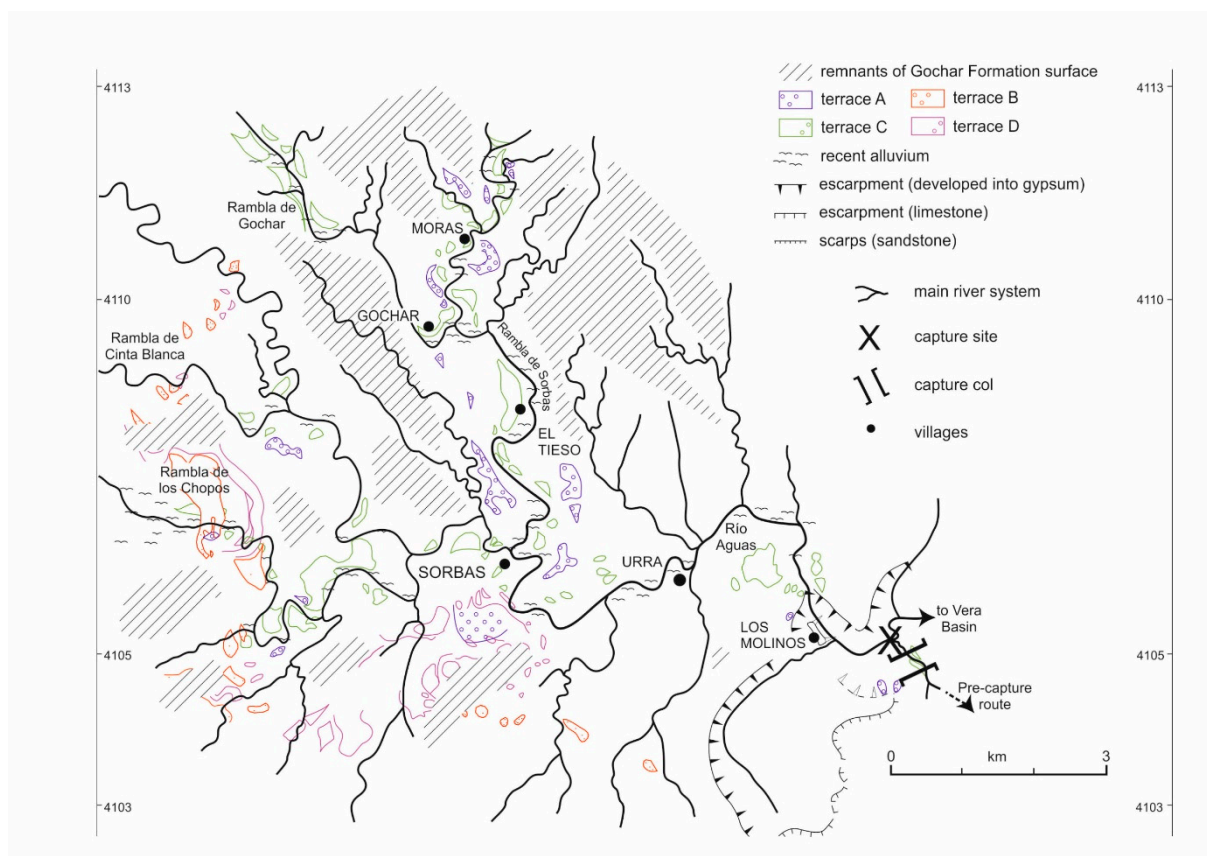
99

100 **Figure 3.** Simplified composite graphic log of the Sorbas Basin sedimentary infill (modified from
 101 [19]) illustrating key stratigraphic units referred to within the text and other figures.

102 The end Zorreras Member is stratigraphically important, being constrained to the Mio-Pliocene
 103 boundary from magnetostratigraphic and biostratigraphic studies [30,31]. Furthermore, the Zorreras
 104 Member lacustrine-marine bands have been used as marker horizons to demonstrate spatially
 105 variable Plio-Quaternary uplift patterns, ranging from 0.08 to 0.16 mm^{a-1} from the basin centre to the
 106 southern margin [19].

107 The overlying Gochar Formation (Figure 3) represents the final infilling stage of the Sorbas Basin,
 108 forming an outcrop of ~80 km² (Figure 2). It comprises a 40-200 m thick conglomerate and sandstone
 109 sequence deposited by alluvial fans and braided rivers [19,20,32] with spatially and temporally
 110 variable degrees of syn- and post-depositional deformation [19]. The fan and river systems are
 111 organised into four distinct drainage systems based on variations in sedimentology, provenance and
 112 palaeocurrent directions [19,20,32]. These drainage systems are important for the morphological
 113 development of the top basin surface, providing a relict topography onto which surface erosion
 114 occurred. The timing of the Gochar Formation is unclear as it lacks any direct age control, with a
 115 broad assignment to the Plio-Quaternary based upon stratigraphic bracketing with the Miocene basin
 116 fill (Zorreras Member) and Pleistocene river terraces.

117 Post Gochar Formation the Sorbas Basin has undergone incision, reflected in the development
 118 of an inset Pleistocene river terrace sequence [24] with coeval landslide, karst and badland
 119 development [33,34]. The river terraces (Figure 4) are configured into up to 5 inset levels (labelled A
 120 to E, where A = highest and oldest and E = lowest and youngest), comprising up to 20 m thick
 121 aggradations of undeformed conglomerate capped by varying degrees of calcrete and soil reddening
 122 dependent on relative age [35].

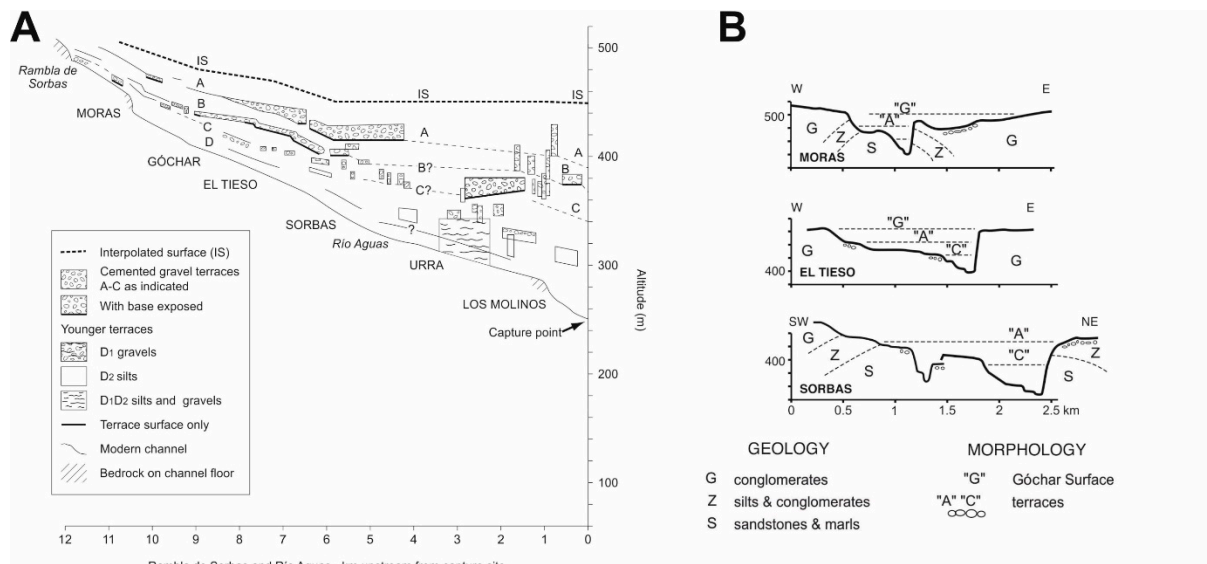


123

124

125 **Figure 4.** Sorbas Basin Middle-Late Pleistocene river terrace map (modified from [10,35]). See Figure
 126 2 for catchment-scale overview.

127 Terrace level A can be inset by up to 20 m into the Gochar Formation sediments (Figure 5), with
 128 the entire terrace sequence recording between 40 m to 160 m of incision between upstream (Moras)
 129 and downstream (Los Molinos) regions [10]. These incision patterns are linked to spatially variable
 130 base level lowering driven by combinations of regional uplift variability and river capture [12,24].
 131 Terrace ages span the Middle-Late Pleistocene based on a range of radiometric and luminescence
 132 techniques [24,36-38]. The terraces are developed along the valleys of the trunk drainage (Río Aguas)
 133 and its major tributaries (Ramblas de Gochar, Moras, Cinta Blanca, los Chopos etc.) (Figure 4).
 134 Terraces have formed within a catchment area of ~285 km² upstream of the Aguas-Feos capture point
 135 (Figures 2, 4 and 5), the site of a major basin-scale capture that occurred ~100 ka, beheading and re-
 136 routing the former southwards flowing drainage (Rambla de los Feos) to the east into the Vera Basin
 137 [24].



138

139 **Figure 5.** A) River long profile and terraces of the (upstream) Rambla de Sorbas and (downstream) 140 Río Aguas (modified from [10]). Marked steps in the Góchar surface and terraces A-C profiles around 141 Sorbas relate to rock strength variations and a change in drainage orientation. B) Cross valley profiles 142 to illustrate the top basin surface (Góchar surface) and its relationship to key inset river terrace levels 143 (modified from [10]).

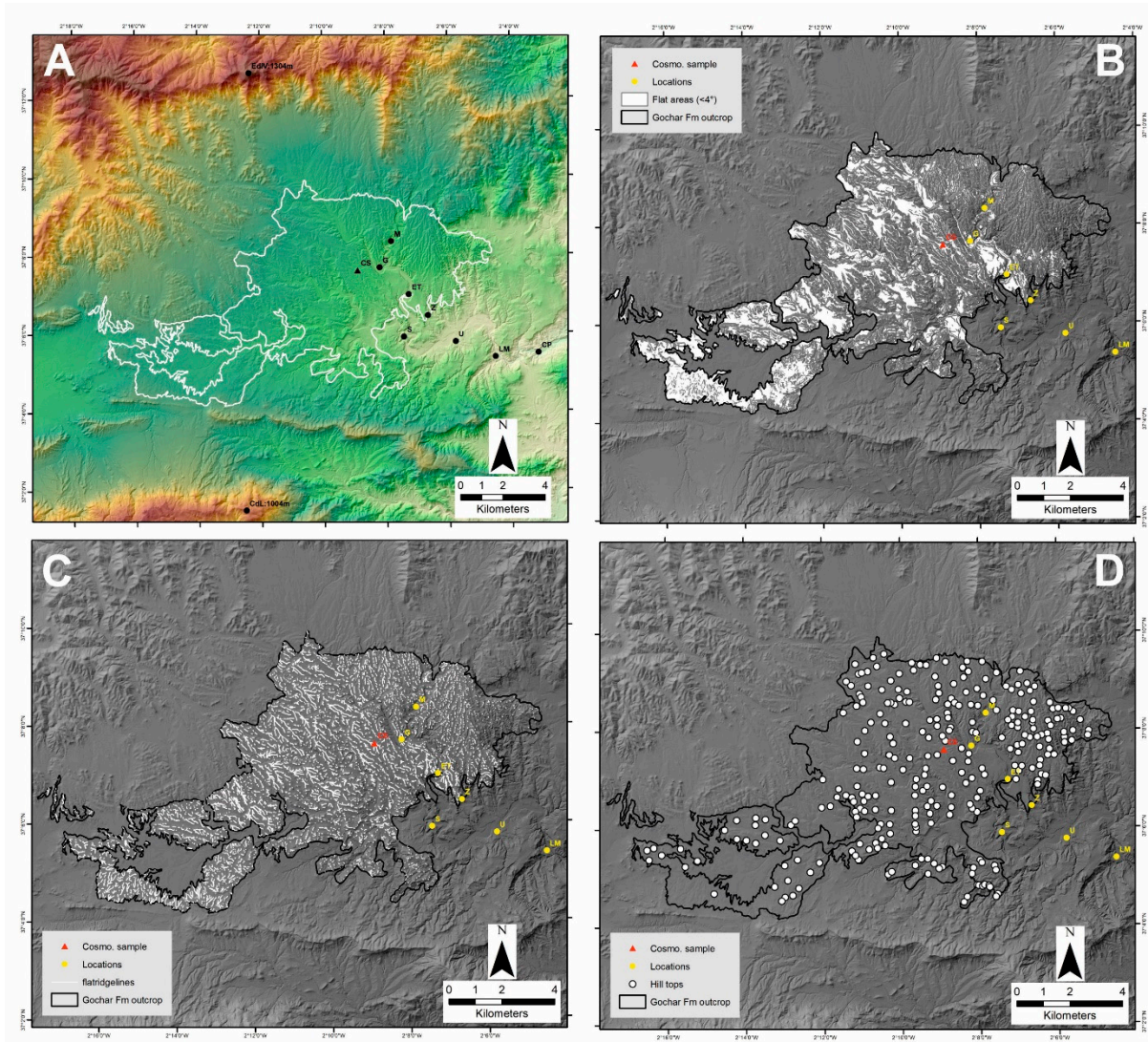
144 The surface studied here is stratigraphically positioned between the Góchar Formation and 145 Level A of the Pleistocene river terrace sequence (Figures 3, 4 and 5) and is likely to be of Quaternary 146 age based on relative dating. Similar high elevation surfaces occur in adjacent intramontane basins 147 (Huércal-Overa, Vera, Tabernas: Figure 1) where they cap the basin fill and mark the onset of basin 148 incision [16,39,40]. Similar surfaces with varying degrees of expression and quality of preservation 149 are noted throughout the Betic Cordillera Internal Zone region where they are considered as an 150 indicator of the most recent phase of relief generation within the Betics [41]. In the Sorbas Basin, the 151 surface is fragmentary but appears to be a single and spatially extensive feature, comprising a series 152 of rounded ridge crests and hilltops, developed primarily onto the Góchar Formation. Here, we focus 153 on the most extensive surface remnants associated with the Góchar Formation outcrop.

154 3. Methods

155 3.1. Surface morphology

156 We describe the top basin surface morphology using a combination of field and remote sensing 157 approaches. The general surface configuration is imaged from different basin margin perspectives 158 using elevated view points and oblique aerial drone imagery. Remote sensing of the surface used 159 digital datasets, interrogated within the ESRI Arc Map 10.5.1 Geographical Information System (GIS). 160 The basin-scale outcrop of the Góchar Formation used digitized 1:50,000 geological maps [25,26]. The 161 broader basin geomorphology used 5 m DEM data sourced online [42] with checks against other 162 commonly used datasets (e.g. SRTM) to ensure visualization and analysis quality [43].

163 The top basin surface is an erosional feature that lacks any sedimentary deposits. As such, the 164 surface remnants are preserved in the rounded ridge crests and hilltops within the highest elevation 165 areas of the Góchar Formation outcrop (Figure 6).



166

167 **Figure 6.** A) DEM and hillshade showing Gochar Formation outcrop and key locations. B) Slope map
 168 of areas of <4°. C) Ridge lines within the Gochar Formation outcrop. D) Final dataset of the highest
 169 elevation hilltops used for surface interpolation.

170 To map these areas, hilltop locations and elevations were combined with flat ridge crest regions.
 171 The assumption is that these highest-flattest ridges are the most representative surface remnants,
 172 since steeper dipping and lower elevation ridges will have been formed by incision into the top basin
 173 surface. Hilltops were extracted from spot heights using scanned 1:25,000 topographic maps [42] in
 174 combination with the 5 m DEM. Hilltops were removed from the dataset if 1) the spot height
 175 coincided with lower level inset river terrace locations (cross-referenced by using a combination of
 176 published terrace maps [35], terrace capping red soil regions identified from satellite imagery, and
 177 cross-valley profiles); 2) had no proximity relationship to the high elevation flat ridge areas (see
 178 below); 3) were anomalously low / high elevation occurrences compared to adjacent spot heights and
 179 4) where the difference between the spot height and DEM elevation value was >5 m. Ridge crests
 180 were obtained from the DEM using an inverse stream extraction approach [44]. A reclassified slope
 181 map was then used to capture the flattest ridges (i.e. ridges coinciding with slopes of <5°). Hilltops
 182 that coincided with the flat ridges were then used as interpolation points from which to reconstruct
 183 the top basin fill surface.

184

185 *3.2. Surface reconstruction and erosion quantification*

186 Digital surface reconstruction is a common geomorphological method for analysis of erosional
187 landscapes at a range of spatial and temporal scales [45-48]. In this study used the variable Inverse
188 Distance Weighting (IDW var) approach [49] due to similarities of basin scale, landscape
189 morphology and higher quality of method statistical performance. Digital points from the cleaned
190 hilltop dataset (see above) were used for the interpolation. The IDW var interpolates between
191 known points giving greater weights to points closest to the prediction location, with weights
192 diminishing with distance away from the known points. The interpolation was extrapolated outside
193 of the Gochar outcrop into the basin margin mountain reliefs to explore the wider configuration of
194 the surface, noting that interpolation accuracy would have diminished due to the nature of IDW var
195 method. The resultant interpolated top basin surface was combined with the modern landscape
196 DEM to allow analysis of areas above and below the interpolated surface (a DEM of Difference). We
197 consider the original top surface to dip towards the basin centre and to have an undulating
198 morphology based on erosion due to lithological and tectonic substrate heterogeneities onto which
199 the surface was developed. Surface hilltops ($n = 278$) within the Gochar Formation outcrop range
200 from 582 m to 442 m with a mean elevation of 511 m and average distance between hilltops of 273
201 m. Elevations between groups of adjacent hilltops is typically <10 m. In areas adjacent to the river
202 valleys the hilltop elevations (i.e. the surface remnants) range from 10-20 m above terrace level A
203 (Figure 5). Thus, a buffer value of $+/-10$ m was used to reclassify the DEM of Difference to model the
204 extent of the top surface that is preserved within the modern landscape.

205 The interpolated top basin surface was used to assess the amount of erosion that has taken place
206 since surface formation. Erosion was calculated by subtracting the interpolated surface from the
207 modern landscape DEM. Since surface formation, the Sorbas Basin catchment area has been modified
208 by capture-related drainage network re-organization [24] and we therefore use the Aguas-Feos
209 capture site as the downstream limit for the erosion calculation.

210 *3.3. Surface dating*

211 Dating of the top basin surface was undertaken using a ^{10}Be - ^{26}Al cosmonuclide depth-profile
212 originally sampled and analysed by [38] as part of a broader chronological investigation of the
213 timing of Quaternary fluvial landscape development within the Sorbas Basin. The paired isotope
214 and depth-profile approach allowed for surface exposure and burial age quantification [50]. The
215 surface exposure technique measures the concentration of cosmonuclides at the surface [51], with
216 concentrations affected by the time of exposure to cosmic radiation, cosmonuclide loss due to
217 erosion, sediment density variability (affects cosmic ray attenuation) and cosmonuclide production
218 variations [52,15]. Burial dating uses known radioactive decay rates of cosmonuclides and requires
219 analysis of samples shielded (deep burial) from cosmic radiation after exposure [53], but with
220 potential problems concerning cosmonuclide inheritance issues related to complex exposure-burial
221 histories prior to deposition [54,55].

222 Sampling was undertaken on a road cutting (37.12692 -2.148214) that passed through one of
223 the higher elevation flat ridges (~495 m) developed into Gochar Formation conglomerates in a
224 north-central basin location (Figure 2). The section comprises ~2.5 m of massive and variably
225 cemented gravel-cobble conglomerate capped by a 0.4 m soil unit, comprising a 0.1 m laminar
226 calcrete and overlying 0.3 m red soil (Munsell = 7.5YR / 4R). Sampling was undertaken up the
227 section face at 0.5 m intervals from 2m depth to the surface with >30 quartz clasts of >5 cm length
228 sampled for each interval. The section location, aspect, angle of section repose, angle to highest
229 topographic feature and surface altitude were quantified for data modelling inputs. The samples
230 were crushed and milled, etched with HF for cleaning followed by dissolution, chemical separation
231 (anion exchange and hydroxide precipitation) and a final metal mixing before AMS measurement.

232 The original age modelling [38] was undertaken using the CRONUS calculator [57] within
233 Matlab. The concentration results revealed no hiatus within the profile so a simple exposure history
234 was explored. This involved using a Chi square minimization method that was applied to the raw
235 nuclide concentration data to allow fitting to the accumulation model equations of [58] with
236 variable inheritance, density and erosion data input values [15,50].

237 For the purpose of this study we remodelled the concentration data using the updated
238 CRONUS 2.3 calculator [59]. New surface erosion estimates of 10m and 4m were inputted to
239 represent the relationship of the cosmogenic sample site to the interpolated surface (see results). A
240 value of 10m was used to reflect the general elevation range between adjacent hilltop heights used
241 for surface interpolation. A value of 4 m was also used as this is the height of the sample site below
242 the interpolated surface. An average upstream altitude of 689 m was derived from the 5 m DEM as
243 a modelling data input to improve the maximum burial age value.

244 Maximum and minimum exposure and burial ages were calculated. These values were
245 considered alongside other published age data for the region to inform on the timing of surface
246 formation. Combination of the remodelled ages with surface incision data enabled amounts and
247 rates of basin erosion to be calculated.

248 4. Results

249 4.1. Surface Morphology and Erosion

250

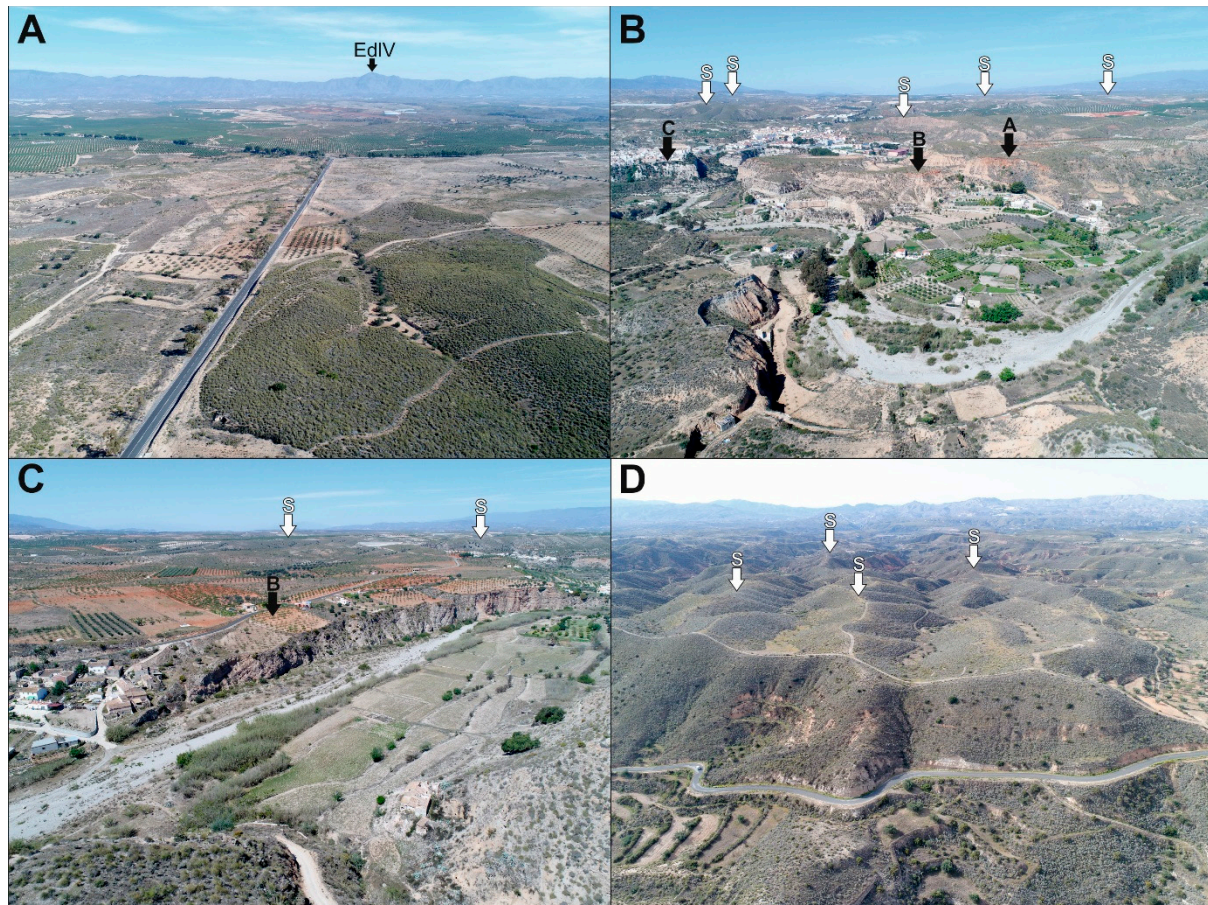
251 The field expression of the surface is shown from a range of basin margin perspectives in Figure
252 7. The surface comprises high elevation isolated hilltops and gently dipping but discontinuous ridge
253 crests, with numerous intervening topographic lows along the ridge lengths and between adjacent
254 hilltops. The hilltops and ridges are further accentuated by incision of the modern drainage network
255 and its tributaries. Despite the erosion, the various landscape panoramic perspectives and along ridge
256 slope profiles (Figure 7) clearly demonstrates a visual correlation and reconstruction of a single
257 surface in a downslope basin centre direction.

258

259 Reconstruction of the surface using IDW var interpolation of the hilltop dataset within the
260 Gochar Formation outcrop shows that the top basin surface is contained almost entirely within the
261 broader sedimentary infill of the Sorbas Basin (Figure 8). The surface is particularly prevalent in
262 northern, central and western regions, with low preservation in the south (Figure 8). Areas eroded
263 below the surface coincide with the modern drainage network, concentrated along the major
264 tributary valleys and becoming widespread towards the east along the Rio Aguas as it routes into the
265 Vera Basin (Figure 9). Other extensive areas below the surface occur in the headwaters of the Tabernas
266 Basin (west) and the Carboneras-Almería Basin (south). Areas above the surface are mainly
267 concentrated in the mountains of metamorphic basement that border the Sorbas Basin, but there are
268 notable areas where Miocene basin fill sediments form topographic highs within the west and south
269 of the basin. Other extensive areas below the surface occur in the headwaters of the Tabernas Basin
270 (west) and the Carboneras-Almería Basin (south). Areas above the surface are mainly concentrated
271 in the mountains of metamorphic basement that border the Sorbas Basin, but there are notable areas
272 where Miocene basin fill sediments form topographic highs within the west and south of the basin.
273 When compared to the modern Río Aguas catchment upstream of the capture site (285 km²), the
274 maximum extent of the interpolated surface covers 144 km², some 50% of the modern catchment. The
275 amounts of incision below the interpolated surface increase downstream to a maximum of -254 m
276 (Figure 9) with a mean basin surface lowering of ~31 m. This incision is concentrated along the lower
277 reaches of tributaries draining to the basin centre and downstream along the main Rio Aguas valley,
278 especially between Sorbas and the capture point east of Los Molinos. The volume of sediment
279 removed by the erosion is 5.95 km³.

280

281

282
283

284 **Figure 7.** Field imaging of relict surface. A: View from south western basin margin (37.06899 -2.19864)
 285 looking north across the basin surface with little dissection. EdIV = Ermita de la Virgen 1304 m. B:
 286 View from southeastern basin margin (37.10498 -2.11419) looking west across the Rambla de Sorbas
 287 inset terrace sequence (A, B, C) in the Sorbas town region. Surface remnants (S) visible in distance. C:
 288 View from eastern basin margin (37.12254 -2.11848) looking northwest across the El Tieso 'B' terrace
 289 with extensive surface remnants visible in far ground (S). D: View south-southwest from the
 290 northeastern basin margin (37.145648 -2.099306) along ridgelines of the relict surface (S).

291

292 The areas of better surface preservation are associated within the confines of the Gochar
 293 Formation outcrop. Within this region, the interpolated surface comprises an area of 35 km², some
 294 44% of the Gochar Formation outcrop. The hilltops, ridges of the interpolated surface and the incised
 295 drainage pick out a series of relict fan-shaped bodies (Figure 10) that broadly correspond to the dip
 296 slopes of the synclinal fold configuration of the Sorbas Basin (Figure 2). These are most evident along
 297 the northern basin margin, comprising at least two fans of 5-6 km length that backfill into the
 298 embayed Sierra de los Filabres mountain front (Figure 10). The clearest of the fans, the eastern
 299 'Cariatz Fan' (Figure 10B), was used by [60] as part of a regional morphometric study of modern and
 300 older Plio-Quaternary fans in SE Spain to illustrate the importance of capture-related re-
 301 organizations of fan source areas.

302
 303
 304

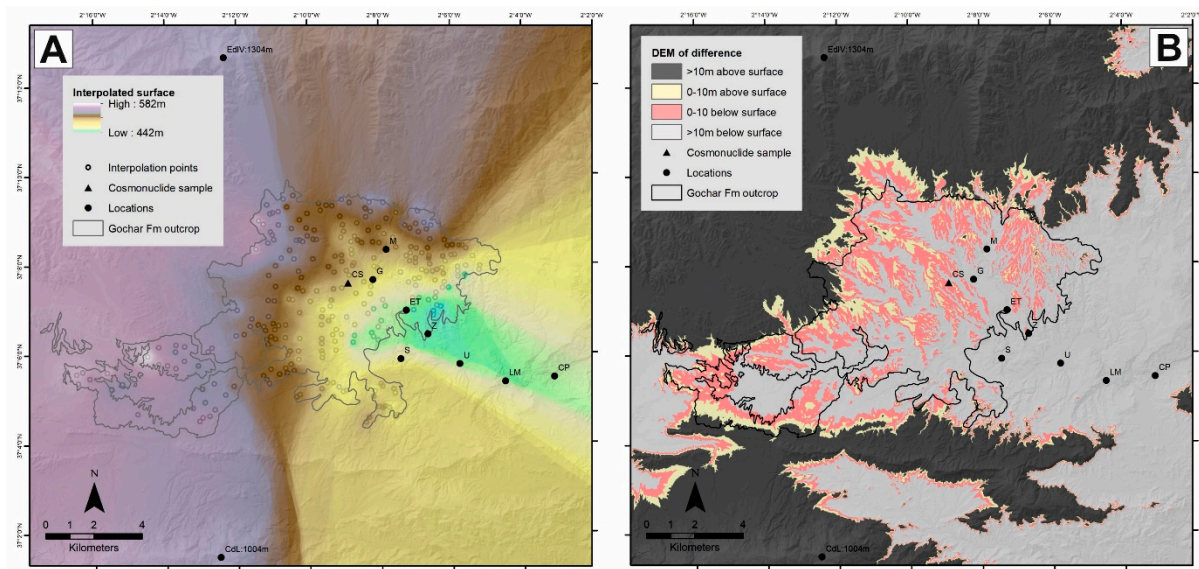


Figure 8. A: Interpolated surface results. B: Comparison of the interpolated surface with the modern landscape highlighting areas that are 10m above and below the interpolated surface.

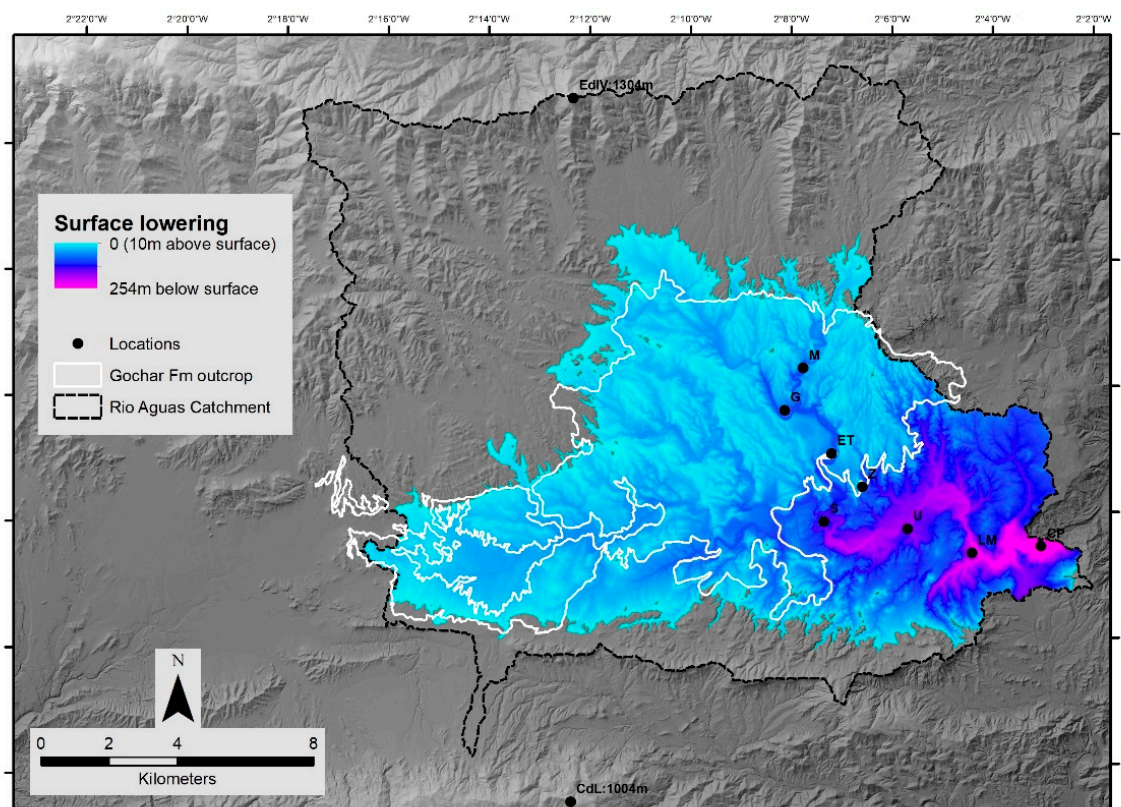
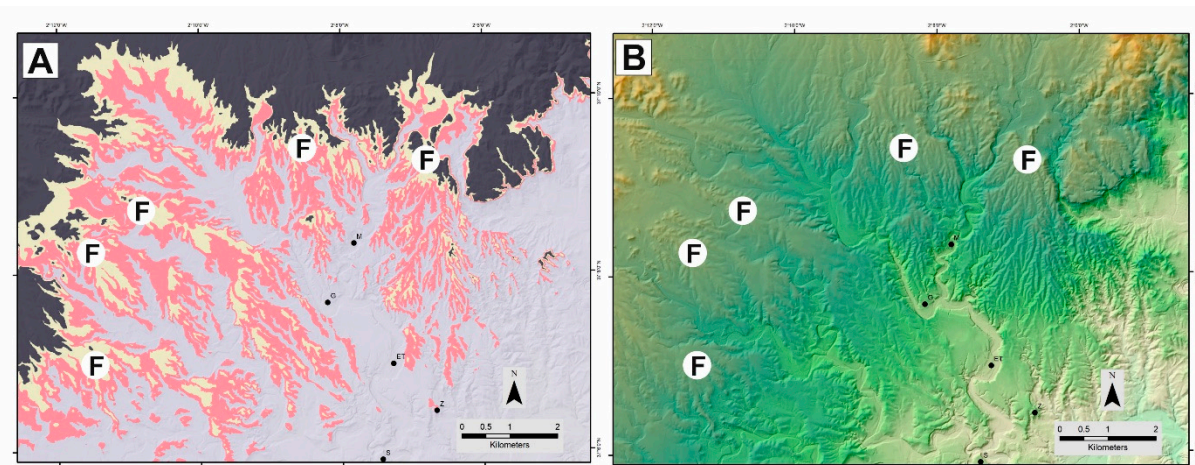


Figure 9. Surface lowering map showing concentrated erosion in the east and upstream along tributary channels.

A series of 4-7 km long fans are also evident along the western and northwestern basin margins, but their morphology is less clear. The surface interpolation (Figure 10) accentuates these fan features suggesting that the formation of the surface erosion and its subsequent incision is accentuating and exploiting the Gochar Formation palaeogeography and its drainage morphology of the Marchalico

319 and Gochar systems [20]. Fan morphologies are not evident in the surface remnants along the
 320 southern basin margin, possibly reflecting a more fragmentary surface record or that the higher uplift
 321 rate and greater degree of deformation along the southern basin margin [61] has destroyed any
 322 Gochar Formation drainage morphology in that area.
 323



324
 325 **Figure 10.** Fan-shaped geometries (F) enhanced by surface interpolation (A). Modern landscape DEM
 326 (B) for comparison. Cariatz Fan = NE fan.
 327
 328

329 4.2. Surface Age and Erosion 330

331 The cosmonuclide sample site location examined by [38] is located on a gently dipping NW-SE
 332 orientated ridge with rounded edges that slope into an adjacent incised drainage network that
 333 visually appears to be part of the relict surface. Within the broader landscape, the sampled ridge is
 334 slightly inset when compared to adjacent ridge hilltop elevations (Figure 11). The interpolation
 335 modelling confirms the inset configuration (Figure 11), with the site occurring at -4m below the
 336 interpolated surface and within the broad -10 m buffer zone (Methods). As such, the sample site does
 337 not provide the best representation of the 'true' surface but instead relates to the onset of incision into
 338 it. However, this incision amount is too small for the sampled ridge to be part of terrace Level A,
 339 which is typically positioned at 20 m below the interpolated surface (Figure 5). A benefit of knowing
 340 surface and terrace elevation variability is that the values provide erosion data inputs for modelling
 341 the cosmonuclide exposure and burial ages (Methods).
 342

343 The remodelled cosmonuclide data are presented in Appendix 1 and summary results in Table
 344 1. Using the higher 10 m erosion value provides exposure ages of 1990 ka (maximum) and 169 ka
 345 (minimum) and burial ages of 1056 ka (maximum) and 679 ka (minimum). In contrast, using a 4 m
 346 erosion value provides exposure ages of 798 ka (maximum) and 169 ka (minimum) and burial ages
 347 of 1048 ka (maximum) and 679 ka (minimum). These ages span the Early-Middle Pleistocene
 348 (maximum exposure-burial ages) and Middle-Late Pleistocene (minimum exposure-burial ages).
 349 Stratigraphic convention should mean that the sediment (burial) age should be older than that of the
 350 surface (exposure) age. However, the age inconsistencies are explainable as they reinforce the surface
 351 origin as an erosional form as opposed to a depositional top basin fill surface. Furthermore, despite
 352 the age variability, the results provide some insight into the broad timing of surface formation. The
 353 minimum 679 ka burial ages suggest that surface is older than 679 ka and probably more in keeping
 354 with the Early Pleistocene. Indeed, the more realistic surface age scenarios are probably closer to the
 355 maximum burial age range 1056-798 ka for both the erosion amount scenarios. An Early Pleistocene
 356 surface age is also supported by the chronologies of the inset river terrace sequence where U-Series
 357 dating of pedogenic terrace capping calcretes show that terraces A and B are Middle Pleistocene
 358 landforms [36,37].

359 **Table 1.** Remodelled cosmonuclide exposure and burial age results. See Supplementary Materials for
 360 detail.

Surface erosion (m)	Min. exposure age (ka)	Max. exposure age (ka)	Min. sediment burial age (Ma)	Max. sediment burial age (Ma)	Min. surface erosion rate (m/Ma)	Max. surface erosion rate (m/Ma)	Min. upstream basin erosion rate (m/Ma)	Max. upstream basin erosion rate (m/Ma)	Reduced chi-square	Min. depositional age (ka)	Max. depositional age (ka)
10	169	1990	0.679	1.048	0.04	5.98	6.8	9.3	2.8	191	1056
4	169	798	0.679	1.048	0.05	5.72	6.6	8.7	2.9	191	798

361
 362 The AMS measurements collectively revealed high concentrations of inherited ^{10}Be and ^{26}Al
 363 (Supplementary Materials) and this begins to inform on the transport history and relative landscape
 364 stability of the end Gochar Formation period prior to surface formation. It suggests that sediments
 365 were generated under low basin erosion rate conditions, implying a relatively stable landscape with
 366 recycling of the basin fill most likely from the Gochar Formation sediments into which the surface
 367 has developed [19].
 368

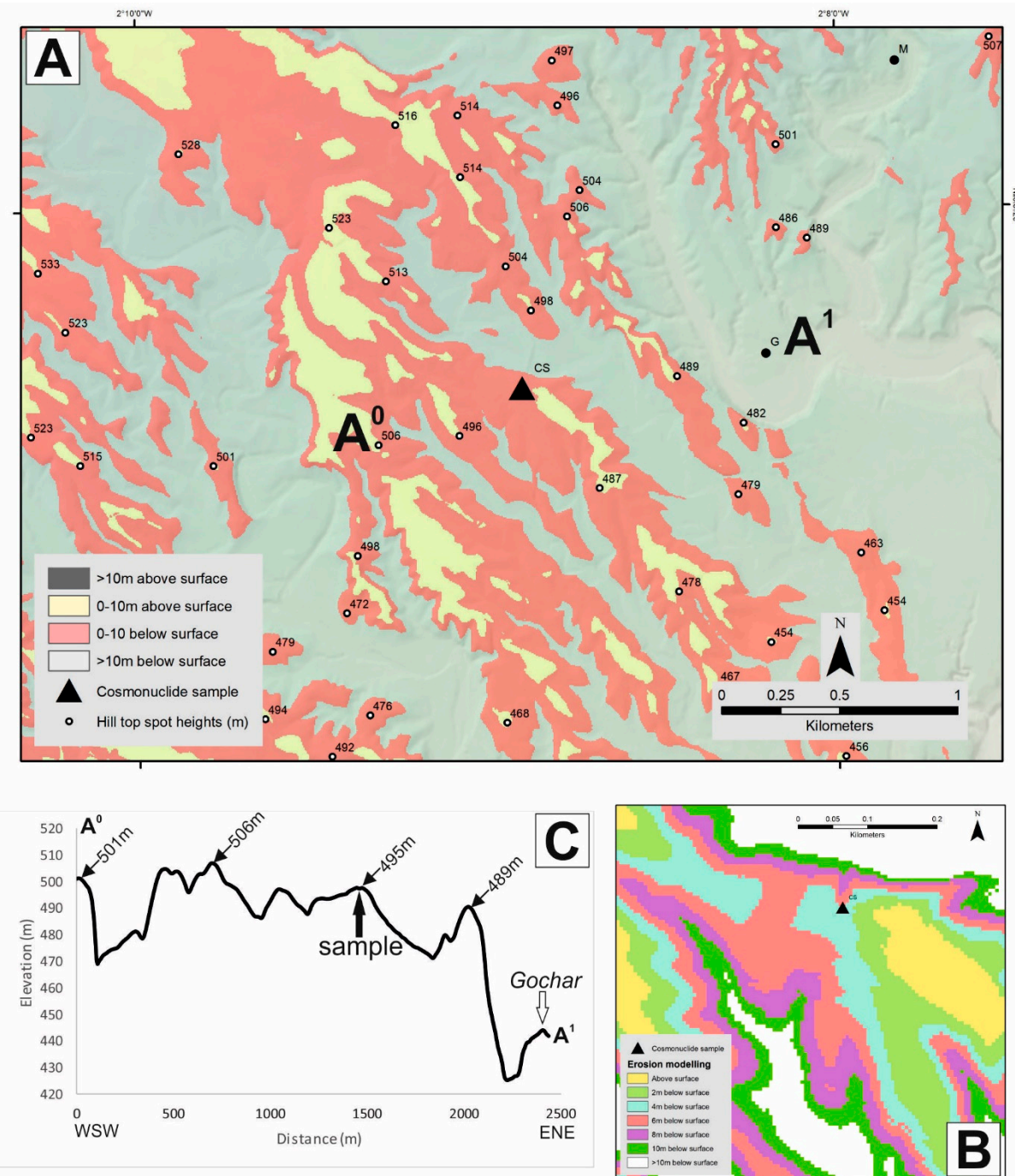
369 The cosmonuclide age data can be combined with the interpolated surface to provide insights
 370 into rates of basin erosion. Because the surface is most likely Early Pleistocene (see above discussion)
 371 we use the maximum and minimum burial ages in conjunction with the surface lowering (~31 m) and
 372 volume (5.95 km³) data to calculate the surface lowering and volume erosion rates. Surface lowering
 373 rates range from 46 mm/ka (minimum burial age: 679 ka) to 29 mm/ka (maximum burial age [10 m]:
 374 1056 ka). Volume rates range from 0.001 km³/ka (minimum burial age: 679 ka) to 0.004 km³/ka
 375 (maximum burial age [10 m]: 1056 ka).
 376

377 5. Discussion

378 5.1 Controls on Surface Formation

379
 380 Despite the fragmentary nature of high elevation hilltops and ridges within the Sorbas Basin,
 381 they link together to form a single surface developed across the basin fill. Its crosscutting relationship
 382 with the underlying Gochar Formation suggests it represents a key basin wide erosional event that
 383 marks the onset of basin incision. The erosion has cut across deformed Gochar Formation sediments,
 384 meaning that surface construction post-dated a basin wide deformation event. Although surface
 385 remnants form a single surface that grades from the basin margins to the basin centre there are local
 386 elevation differences between adjacent surface remnants. These differences may relate to variations
 387 in strength, stratigraphy and localised deformation of the basin fill or a passive exploitation of the
 388 basin fill palaeogeography and its relict morphology of the depositional environment. For example,
 389 surfaces developed into flat lying and fine grained lacustrine dominated intramontane basin infills
 390 (e.g. Guadix-Baza [11]) are more likely to be well developed and spatially extensive than those
 391 developed into dipping and coarse-grained alluvial intramontane basin fills (this study).

392

393
394

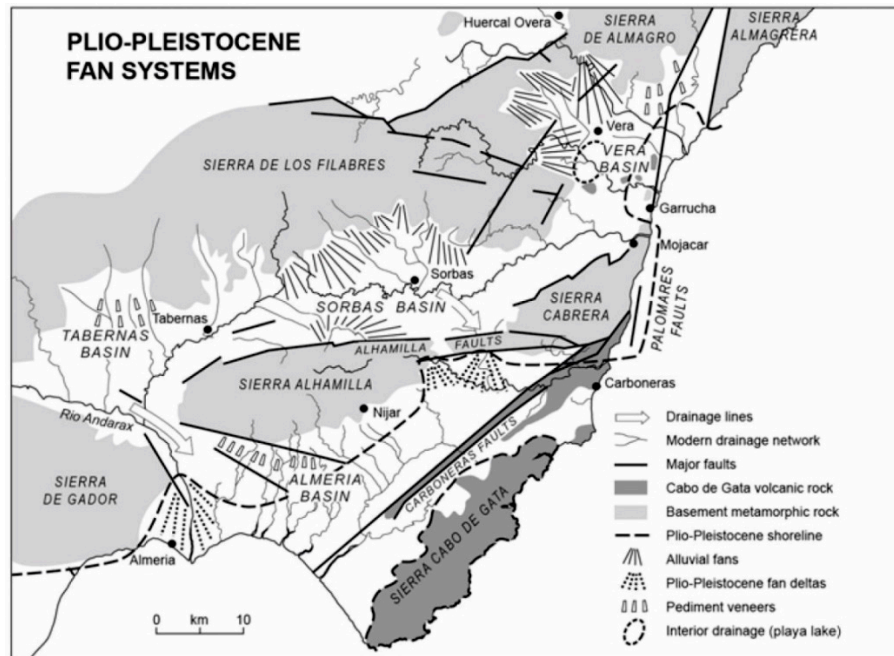
395 **Figure 11.** Visualization of the interpolated surface at 10 m (A) and 2 m (B) intervals, showing that
 396 the cosmonuclide sample site is located ~4 m below the interpolated surface. C) Topographic profile
 397 further illustrating the inset nature of sample site.

398

399 Surfaces are evident throughout Betic Cordillera intramontane basins (Figure 12), occupying
 400 mountain fronts where surface remnants dip towards the basin centre [13]. These surfaces are either
 401 1) degraded forms, lacking in sediment cover and developed onto the Plio-Pleistocene continental
 402 alluvial basin infill (e.g. Sorbas Basin) or 2) are well preserved, with a <20 m thick cover of coarse-
 403 grained alluvial conglomerates, that unconformably overlie Neogene marine basin infill (e.g.
 404 Tabernas and eastern Vera Basin) (Figure 12). The well-preserved surfaces often comprise a
 405 pedogenic calcrete cap, with groundwater calcretes sometimes developed along the basal
 406 unconformity contact [14,62]. Although surfaces may have origins associated with alluvial fan

407 environments [13], they are more typical of pediments (*sensu* [63]) that have been observed
 408 worldwide, with examples throughout SE Spain often referred to using the French term 'glaci' [64].
 409 The degraded surface considered here could be a highly eroded pediment remnant, most likely a
 410 bedrock pediment or the remnants of the bedrock base of a pediment due to absence of calcrete and
 411 alluvial cover. Studies of pediment formation [65] suggest they form at mountain fronts where
 412 bedrock weathers to sediment; in climates with a soil hydrology, vegetation cover and weathering
 413 style that suppresses fluvial incision and deep bedrock weathering; and a balanced mountain front
 414 sediment flux and base-level position. If the top basin surface follows these criteria for autogenic
 415 formation, then the surface informs indirectly on Quaternary climate and tectonics. The climatic
 416 criteria are fulfilled due to a persistence of seasonally variable cool/warm dryland climatic conditions
 417 throughout the Quaternary [66-69]. However, the base-level configuration has changed, particularly
 418 with respect to the top basin surface as it marks a key point at which the basin switches from
 419 sedimentation to erosion, after which there is a sustained base-level lowering linked to tectonic uplift
 420 and capture [14,70]. For the top surface to form as a basin wide feature means that dryland conditions
 421 must have coincided with a stable and sustained basin level position during a time of relative tectonic
 422 quiescence and a time when the drainage network configuration was not conducive to capture. Uplift
 423 rate quantifications for the Sorbas Basin are time averaged from the lower Pliocene (70-160 m Ma⁻¹;
 424 [19,70] and thus lack temporal clarity to inform on the restricted pediment formation timescale.
 425 However, direct evidence for deformation is restricted to the Gochar Formation sediments into which
 426 the surface is developed, implying a marked reduction in tectonic activity at the time of surface
 427 formation and thus base level stabilization. Tectonics would have also played a passive role in surface
 428 formation, with the overall basin syncline configuration forming fold limb dip slope drainages routed
 429 to a basin centre axial drainage coincident with the basin syncline axis. Subsequent fluvial incision
 430 appears to have concentrated along the synclinal axis, dissipating upstream along the fold limb
 431 configured streams (Figures 8 and 9). The passive influence of fold structures on drainage pattern
 432 configuration and development is a commonly reported feature in collisional mountain belt settings
 433 [71].

434

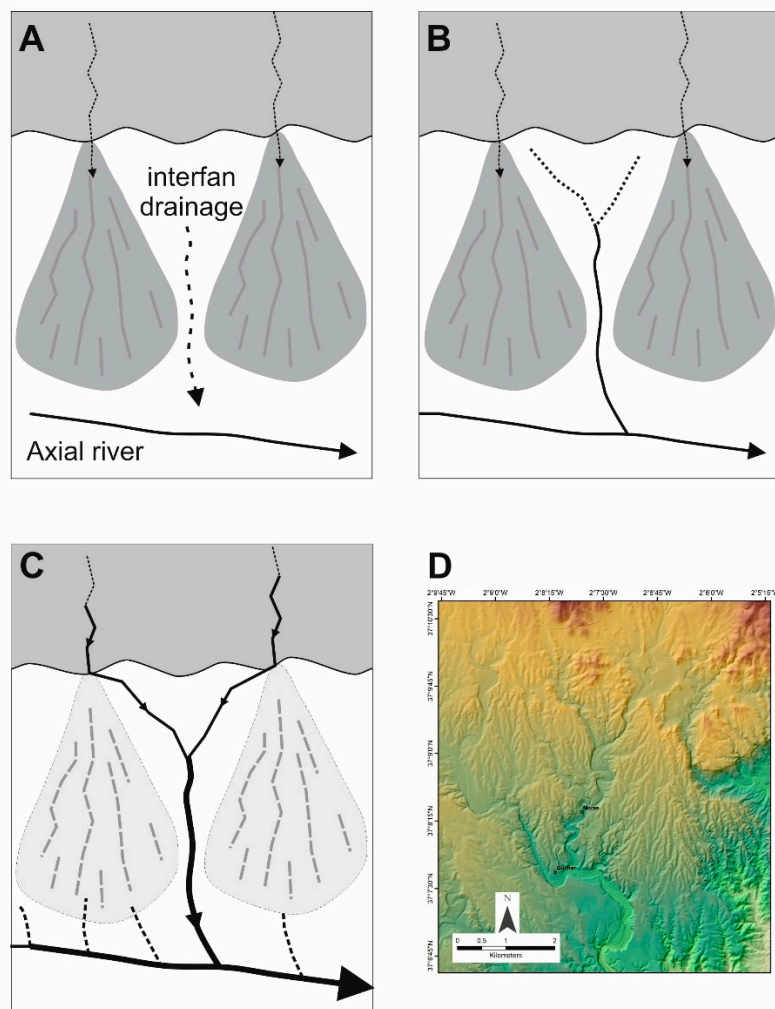


435

436 **Figure 12.** Regional occurrence of Plio-Pleistocene alluvial fan / pediment systems within the east-
 437 central Betic Cordillera [13]. Degraded surfaces are developed onto Plio-Pleistocene continental
 438 (alluvial fan) sediments, whilst well preserved surfaces (pediment veneers) are developed onto
 439 Neogene marine sediments.

440

441 The very nature of the surface as a continuous basin wide feature implies the absence of an
 442 incised drainage network for it to form by autogenic processes e.g. [64]. Drainage routing throughout
 443 the Plio/Quaternary has recorded a persistent pattern of basin margin streams feeding an axial
 444 drainage [12,20,24]. Because the surface has formed as an interval in-between the final basin infilling
 445 and pre-basin incision, it too is likely to have formed by the same basin convergent drainage pattern
 446 (Figure 12). If the basin was undissected then radiating streams with collective fan-shaped forms
 447 would have dominated the palaeogeography (in-keeping with the Gochar Formation), with
 448 autogenic lateral shifting of the radiating streams being responsible for creating the pediment like
 449 surface, noting that any pediment cover sediments are not preserved due to the eroded / degraded
 450 surface form. The surface remnants and interpolation mapping (Figure 10) provides strong evidence
 451 for large fan-shaped bodies along the northern and western basin margins. These morphologies,
 452 particularly along the northern margin, are accentuated because of progressive surface incision and
 453 localized captures.
 454



455
 456 **Figure 13.** Fan / pediment abandonment model based on Sorbas Basin northern margin. A-C =
 457 interfan development and capture of mountain front fan feeder streams. D = relict fan morphology
 458 with former interfan drainage now forming a key component of the current drainage network.
 459

460 Headwards erosion by the axial drainage has exploited the inter-fan drainage areas (Figure 13).
 461 It is common for alluvial fans to develop an incised drainage along their axial feeder channel due to
 462 a connectivity interplay between fan head and fan toe base-level variations [72]. Because incision and
 463 headwards erosion has been concentrated along the interfan areas it suggests that the fans responsible
 464 for autogenically creating the surface were undissected with insufficient axial drainage to be
 465 exploited. As headwards erosion has proceeded up the interfan areas it has captured the fan feeders,

466 resulting in fan abandonment [73]. The fans forming the pediment surface would have also possessed
467 an overall convex morphology with topographic lows present within interfan areas. This convex
468 morphology may have also played a role in passively influencing interfan drainage exploitation.
469

470 5.2. *Timing of surface formation*

471
472 The remodelled cosmonuclide data suggest that the surface is an Early Pleistocene feature, with
473 the max-min burial ages (1056-679 ka: Table 1) providing the most coherent age range indicators for
474 surface development. This means that the underlying Gochar Formation into which the surface is
475 developed spans the Pliocene and probably the earliest Pleistocene based upon bracketing between
476 a basal Mio-Pliocene boundary age [30] and a top Early Pleistocene age (this study). From a geological
477 perspective the Early Pleistocene surface age presented here is significant for understanding the Late
478 Miocene geological history of the Sorbas Basin which has received considerable attention for its role
479 in documenting the Mediterranean Messinian Salinity Crisis. [31] describe the same surface studied
480 here (see their Fig. 8G and Fig 7C of this study) as a fan-delta abandonment feature assigning a Mio-
481 Pliocene (~5.3 Ma) boundary age to the surface through downslope extrapolation to a
482 biostratigraphically dated Zorreras Member type location section, the Zorreras Hill (Figure 2). This
483 450 m elevation hilltop is capped by Gochar Formation conglomerates and fits within our
484 interpolated surface dataset. However, its Early Pleistocene cosmonuclide age bears no relationship
485 to the immediate post Messinian Salinity Crisis recovery of the Sorbas basin as implied by [31].
486

487 The regional significance of the style and timing of Sorbas Basin surface formation within the
488 Betic Cordillera can be further explored through comparison with adjacent intramontane basins
489 (Figure 12). To the east, the Vera Basin is like Sorbas, comprising a deformed continental basin infill
490 (Salmerón Formation) that grades into a high elevation pediment surface and an inset fan pediment-
491 river terrace sequence [74-76]. Electron Spin Resonance (ESR) dating brackets the Salmerón
492 Formation and its pediment to the Early Pleistocene (~2.4-1.3 Ma) [77,78]. The timing appears co-eval
493 with the latter stages of the Gochar Formation, attributed to regional uplift timing and amount
494 variability between the Sorbas (earlier and greater uplift) and Vera Basins [40]. The inset Vera Basin
495 pediment-river terrace sequence spans the Middle to Late Pleistocene based upon ESR and OSL
496 chronologies [79,80]. This timing is in-keeping with the U-Series dated Middle-Late Pleistocene
497 Sorbas Basin river terrace sequence [36,37]. Other adjacent basins (Huércal-Overa, Tabernas,
498 Carboneras-Almería) show varying degrees of geological-geomorphological similarity: 1) Pliocene-
499 Early Pleistocene basin fill, 2) Early Pleistocene deformation and 3) Middle-Late Pleistocene
500 pediment-river terrace sequence formation [16,39,50]. [41] attributes the Early Pleistocene to the most
501 recent phase of Betic Cordillera relief generation, highlighting a poorly understood interplay between
502 mechanical and isostatic relief building processes, with ductile crustal flow cited as a key
503 Plio/Quaternary uplift mechanism. Of note, is the Guadix-Baza Basin, the largest and most
504 intensively studied intramontane basins in the region. This basin occupies a central-interior location
505 within the Betics and differs in timing to Sorbas and its adjacent basins. The Guadix-Baza Basin is
506 characterised by a continuous Miocene-Late Pleistocene continental sedimentary infill [69], capped
507 by a single Late Pleistocene pediment into which extensive basin wide erosion has occurred following
508 capture by the Río Guadalquivir sometime between 350 to 68 ka [4,48]. This difference in timing and
509 pattern of basin geological-geomorphological development reflects variations and connectivity of
510 regional base-levels. Sorbas and adjacent basins occupy marginal mountain belt locations with better
511 connectivity to the Mediterranean coastlines, thus responding more effectively to regional base-level
512 change. In contrast, the Guadix-Baza Basin has an interior mountain belt location with an internal
513 drainage disconnected from regional base-level variability, until captured very recently geologically
514 speaking.
515

516 High elevation Early Pleistocene pediment surfaces are also present within intraplate basins as
517 part of the largest drainage systems in Iberia such as the Duero and Tajo [81]. These surfaces have

518 alluvial fan origins and show development within wide-shallow valleys that form the beginnings of
519 river terrace staircases that record hundreds of metres of incision [81]. Thus, the Early Pleistocene is
520 an important interval for surface development and a key marker for subsequent fluvial landscape
521 incision, both within the Betic Cordillera (this study) and within Iberia [82]. Climate and base level
522 (tectonic and capture) variability are widely cited controlling mechanisms for Early Pleistocene
523 Iberian landscape development [48, 81-83]. Surface formation within the Sorbas Basin clearly
524 demonstrates interplay of these factors, but the surface itself probably reflects a sustained period of
525 climate stability and base level position to allow the surface to form autogenically at a basin scale.
526 Marked changes to the global climate [84] and regional base levels [12,41] are then driving the surface
527 abandonment and incision.

528

529 5.3 Basin Erosion

530

531 The interpolation derived basin erosion rates quantified in this study (Figure 9) can be compared
532 with erosion of the Sierra de los Filabres using ^{10}Be [85]. Rates of 52 ± 6 mm/ka were derived from
533 basement schist dominated catchments of tributaries to the Río Jauto along the northeastern margin
534 of the Sorbas Basin [85]. These catchments were formerly part of the main Sorbas Basin drainage
535 before being captured and routed to the southern Vera Basin sometime during the Middle-Late
536 Pleistocene [12]. The average basin surface lowering rates calculated in this study using the dated
537 interpolated surface cover a lower range at 29-46 mm/ka. This could be due to rock strength
538 differences between variably cemented conglomerate basin infill (this study) vs easily weathered
539 basement schist [85]. However, the low value from the Sorbas surface is still broadly in keeping with
540 Betic Cordillera mean (64 ± 54 mm/ka $^{-1}$), reflecting low tectonic uplift and possibly a steady state
541 topography where denudation balances uplift [85].

542 **6. Conclusions**

- 543 • Despite a fragmentary nature, the top Sorbas Basin surface can be reconstructed using GIS
544 interpolation (IDW var) where a sufficiently high-resolution DEM is available;
- 545 • The surface is an erosional form and not the depositional surface of the Gochar Formation;
- 546 • The surface is an Early Pleistocene feature, developed onto deformed basin fill;
- 547 • The surface reconstruction approach used here could be used to inform on sampling strategy for
548 dating or could help clarify local surface erosion for age modelling purposes;
- 549 • The basin wide configuration of the surface suggests surface formation by autogenic processes
550 that are operating within a stable landscape characterized by a sustained dryland climate and
551 fixed base-level;
- 552 • The relict fan-morphology picked out by the surface remnants suggests the surface was
553 autogenically eroded by undissected radiating mountain front streams that formed fan-shaped
554 bodies;
- 555 • The Early Pleistocene surface age helps stratigraphically bracket the underlying Gochar
556 Formation to the Pliocene. This clarifies the degraded pediment surface as a Quaternary
557 landscape feature and not a Mio-Pliocene fan delta abandonment surface linked to the post
558 Messinian salinity crisis recovery;
- 559 • Surface abandonment took place during the Middle Pleistocene with preferential incision along
560 interfan drainage lines, resulting in capture to preserve the relict fan morphologies;
- 561 • Early Pleistocene surfaces are evident throughout Betic Cordillera intramontane basins as either
562 1) well developed pediments, developed onto Neogene marine basin fill sediments (e.g.
563 Tabernas, Vera Basins) or 2) degraded pediments developed onto Plio-Pleistocene continental
564 alluvial basin fill sediments (Sorbas Basin). Collectively these pediments are regionally and
565 temporally significant, with formation occurring during a stable phase that post-dates
566 deformation of the Plio-Pleistocene continental sediments that form the final basin infill. The
567 deformation and subsequent surface formation probably correspond to the most recent major
568 uplift and relief building phase of the Betic Cordillera;

569 • Surface form reflects differences in substrate lithology, passive basin tectonic configuration and
570 depositional setting (e.g. lake vs fan);
571 • Regional variations in surface preservation and differences in formation timing relates to base-
572 level connectivity with the Mediterranean coastal margins of the Betic Cordillera;
573 • Surface lowering and erosion amounts, and rates are low, comparing well with other denudation
574 techniques (e.g. ^{10}Be) and are in keeping with the Betic Cordillera as a low uplift rate mountain
575 range. The base-level lowering since surface formation is probably an ongoing response to the
576 low uplift rates and basin scale capture events.

577 **Supplementary Materials:** The following are available online, Figures S1-S4: cosmonuclide results graphs for
578 4m erosion scenario, Figures S5-S8: cosmonuclide results graphs for 10m erosion scenario , Tables S1-S7:
579 cosmonuclide datasets for 4m erosion scenario, Tables S8-S14: cosmonuclide datasets for 10m erosion scenario.

580 **Author Contributions:** Conceptualization, MS and AEM; Methodology, MS, AEM, AR, SL; Software, AR, SL.;
581 Validation, MS, AR, SL; Formal Analysis, MS, AR, SL; Investigation, MS, AEM, AR, SHK, SL; Resources, AR, SL;
582 Data Curation, MS, AR.; Writing – Original Draft Preparation, MS; Writing – Review & Editing, AEM, AR, SHK,
583 SL; Visualization, MS; Supervision, MS; Project Administration, MS; Funding Acquisition, MS.

584 **Funding:** This research was part funded by NERC grants CIAF 9039-1007 and NE/F00642X/1.

585 **Acknowledgments:** Thanks to Lindy Walsh and Paco Contreras of the Cortijo Urra Field Centre (Sorbas) for
586 fieldwork support.

587 **Conflicts of Interest:** "The authors declare no conflict of interest."

588

589 **References**

- 590 1. Kingston, D.R.; Dishroon, C.P.; Williams, P.A. Global basin classification system. *AAPG Bull.* **1983**,
591 pp.2175-2193.
- 592 2. Sanz De Galdeano, C.; Vera, J.A. Stratigraphic record and palaeogeographical context of the Neogene
593 basins in the Betic Cordillera, Spain. *Basin Res.* **1992**, *4*, pp. 21-35.
- 594 3. Sobel, E.R.; Hilley, G.E.; Strecker, M.R. Formation of internally drained contractional basins by aridity-
595 limited bedrock incision. *J. Geophys. Res.* **2003**, *108*(B7). <https://doi.org/10.1029/2002JB001883>
- 596 4. Calvache, M.L.; Viseras, C. Long-term control mechanisms of stream piracy processes in southeast
597 Spain. *Ear. Sur. Proc. and Land.* **1997**, *22*, pp.93-105.
[https://doi.org/10.1002/\(SICI\)1096-9837\(199702\)22:2%3C93::AID-ESP673%3E3.0.CO;2-W](https://doi.org/10.1002/(SICI)1096-9837(199702)22:2%3C93::AID-ESP673%3E3.0.CO;2-W)
- 598 5. Craddock; W.H., Kirby, E.; Harkins, N.W.; Zhang, H.; Shi, X.; Liu, J. Rapid fluvial incision along the
599 Yellow River during headward basin integration. *Nat. Geosci.* **2010**, *3*, p.209.
- 600 6. Soria, J.M.; Fernández, J.; Viseras, C. Late Miocene stratigraphy and palaeogeographic evolution of the
601 intramontane Guadix Basin (Central Betic Cordillera, Spain): implications for an Atlantic-
602 Mediterranean connection. *Palaeogeog. Palaeoclim. Palaeoec.* **1999**, *151*, pp.255-266.
[https://doi.org/10.1016/S0031-0182\(99\)00019-X](https://doi.org/10.1016/S0031-0182(99)00019-X)
- 603 7. Benvenuti, M.; Bonini, M.; Moroni, A. Tectonic control on the Late Quaternary hydrography of the
604 Upper Tiber Basin (Northern Apennines, Italy). *Geomorphology* **2016**, *269*, pp.85-103.
<https://doi.org/10.1016/j.geomorph.2016.06.017>
- 605 8. Watchman, A.L.; Twidale, C.R. Relative and 'absolute' dating of land surfaces. *Earth-Sci. Rev.* **2002**, *58*,
606 pp.1-49. [https://doi.org/10.1016/S0012-8252\(01\)00080-0](https://doi.org/10.1016/S0012-8252(01)00080-0)
- 607 9. Viseras, C.; Fernández, J. Sedimentary basin destruction inferred from the evolution of drainage
608 systems in the Betic Cordillera, southern Spain. *J. Geol. Soc., Lon.* **1992**, *149*, pp. 1021-1029.
<https://doi.org/10.1144/gsjgs.149.6.1021>
- 609 10. Stokes, M.; Mather, A.E.; Harvey, A.M. Quantification of river-capture-induced base-level changes and
610 landscape development, Sorbas Basin, SE Spain. *Geol. Soc., Lon., Spec. Pub.* **2002**, *191*, pp.23-35.
<https://doi.org/10.1144/GSL.SP.2002.191.01.03>
- 611 11. García-Tortosa, F.J.; Alfaro, P.; de Galdeano, C.S.; Galindo-Zaldívar, J. Glacis geometry as a
612 geomorphic marker of recent tectonics: The Guadix–Baza basin (South Spain). *Geomorphology* **2011**, *125*,
613 pp.517-529.
<https://doi.org/10.1016/j.geomorph.2010.10.021>
- 614 12. Harvey, A.M.; Whitfield, E.; Stokes, M.; Mather, A. The Late Neogene to Quaternary Drainage
615 Evolution of the Uplifted Neogene Sedimentary Basins of Almería, Betic Chain. In *Landscapes and
616 Landforms of Spain*, Gutiérrez F., Gutiérrez M. Eds.; Springer, Dordrecht: The Netherlands 2014; pp. 37-
617 61 ISBN 978-94-017-8628-7
- 618 13. Harvey, A.M.; Stokes, M.; Mather, A.; Whitfield, E., Spatial characteristics of the Pliocene to modern
619 alluvial fan successions in the uplifted sedimentary basins of Almería, SE Spain: review and regional
620 synthesis. *Geol. Soc., Lond., Spec. Pub.* **2018**, *440*, pp.SP440-5. <https://doi.org/10.1144/SP440.5>
- 621 14. Stokes, M.; Nash, D.J.; Harvey, A.M. Calcrete 'fossilisation' of alluvial fans in SE Spain: The roles of
622 groundwater, pedogenic processes and fan dynamics in calcrete development. *Geomorphology* **2007**,
623 85(1-2), pp.63-84. <https://doi.org/10.1016/j.geomorph.2006.03.020>
- 624 15. Rodés, Á.; Pallàs, R.; Braucher, R.; Moreno, X.; Masana, E.; Bourlés, D.L. Effect of density uncertainties
625 in cosmogenic ¹⁰Be depth-profiles: dating a cemented Pleistocene alluvial fan (Carboneras Fault, SE
626 Iberia). *Quat. Geochron.* **2011**, *6*, pp.186-194. <https://doi.org/10.1016/j.quageo.2010.10.004>
- 627 16. Geach, M.R.; Thomsen, K.J.; Buylaert, J.P.; Murray, A.S.; Mather, A.E.; Telfer, M.W.; Stokes, M. Single-
628 grain and multi-grain OSL dating of river terrace sediments in the Tabernas Basin, SE Spain. *Quat.*
629 *Geochron.* **2015**, *30*, pp.213-218. <https://doi.org/10.1016/j.quageo.2015.05.021>
- 630 17. Martín, J.; Braga, J.C. Messinian events in the Sorbas Basin in southeastern Spain and their implications
631 in the recent history of the Mediterranean. *Sed. Geol.* **1994**, *90*, pp.257-268.
[https://doi.org/10.1016/0037-0738\(94\)90042-6](https://doi.org/10.1016/0037-0738(94)90042-6)
- 632 18. Haughton, P.D. Deposits of deflected and ponded turbidity currents, Sorbas Basin, southeast Spain. *J.*
633 *Sed. Res.* **1994**, *64*, pp. 233-246.
- 634 19. Mather, A.E., 1991, Cenozoic drainage evolution of the Sorbas Basin SE Spain. PhD Thesis, University
635 of Liverpool, Liverpool, 1991.

643 20. Mather, A.E.; Harvey, A.M., 1995. Controls on drainage evolution in the Sorbas basin, southeast Spain.
644 In *Mediterranean Quaternary River Environments*, Lewin, J., Macklin, M.G., Woodward, J.C. Eds.;
645 Balkema: Rotterdam, The Netherlands, 1995, pp. 65–75. ISBN 9054101911

646 21. IGME, Mapa de Geologico de España, 1:200 000. Almería-Garrucha, 84–85, Madrid, 1980, 2nd Edition.

647 22. IGME, Mapa de Geologico de España, 1:200 000. Baza, 78. Madrid, 1983, 2nd Edition.

648 23. IGME, Mapa de Geologico de España, 1:200 000. Murcia, 78. Madrid, 1983, 2nd Edition.

649 24. Harvey, A.M.; Wells, S.G. Response of Quaternary fluvial systems to differential epeirogenic uplift:
650 Aguas and Feos river systems, southeast Spain. *Geology* **1987**, *15*, 689–693.

651 25. IGME, Mapa de Geologico de España, 1:50 000. Sorbas, 1031, 24–42, Madrid, 1973.

652 26. IGME, 1973. Mapa de Geologico de España, 1:50 000. Tabernas, 1030, 23–42, Madrid 1973.

653 27. Vázquez, M.; Jabaloy, A.; Barbero, L.; Stuart, F.M. Deciphering tectonic-and erosion-driven
654 exhumation of the Nevado-Filábride Complex (Betic Cordillera, Southern Spain) by low temperature
655 thermochronology. *Terra Nova* **2011**, *23*, pp.257-263. <https://doi.org/10.1111/j.1365-3121.2011.01007.x>

656 28. Platt, J.P.; Kelley, S.P.; Carter, A.; Orozco, M. Timing of tectonic events in the Alpujárride Complex,
657 Betic Cordillera, southern Spain. *J. Geol. Soc. Lon.* **2005**, *162*(3), pp.451-462.
658 <https://doi.org/10.1144/0016-764903-039>

659 29. Giacconi, F.; Booth-Rea, G.; Martínez-Martínez, J.M.; Azañón, J.M.; Pérez-Peña, J.V; Pérez-Romero,
660 J.; Villegas I. Geomorphic evidence of active tectonics in the Sierra Alhamilla (eastern Betics, SE Spain).
661 *Geomorphology* **2012**, *145*, pp. 90-106. <https://doi.org/10.1016/j.geomorph.2011.12.043>

662 30. Martín-Suárez, E.; Freudenthal, M.; Krijgsman, W.; Fortuin, A.R. On the age of the continental deposits
663 of the Zorreras Member (Sorbas Basin, SE Spain). *Geobios* **2000**, *33*, pp.505-512.

664 31. Clauzon, G.; Suc, J.P.; Do Couto, D.; Jouannic, G.; Melinte-Dobrinescu, M.C.; Jolivet, L.; Quillévéré, F.;
665 Lebret, N.; Mocochain, L.; Popescu, S.M.; Martinell, J. New insights on the Sorbas Basin (SE Spain): the
666 onshore reference of the Messinian Salinity Crisis. *Mar. Pet. Geo.* **2015**, *66*, pp.71-100.
667 <https://doi.org/10.1016/j.marpetgeo.2015.02.016>

668 32. Mather, A.E. Basin inversion: some consequences for drainage evolution and alluvial architecture.
669 *Sedimentology* **1993** *40*, 1069-1089. <https://doi.org/10.1111/j.1365-3091.1993.tb01380.x>

670 33. Griffiths, J.S.; Hart, A.B.; Mather, A.E.; Stokes, M. Assessment of some spatial and temporal issues in
671 landslide initiation within the Río Aguas Catchment, South-East Spain. *Landslides* **2005**, *2*, pp.183-192.

672 34. Mather, A.E.; Stokes, M.; Griffiths, J.S. Quaternary landscape evolution: a framework for
673 understanding contemporary erosion, southeast Spain. *Land Deg. Dev.* **2002**, *13*, pp.89-109.
674 <https://doi.org/10.1002/ldr.484>

675 35. Harvey, A.M.; Miller, S.Y.; Wells, S.G. Quaternary soil and river terrace sequences in the Aguas/Feos
676 river systems: Sorbas basin, southeast Spain. In *Mediterranean Quaternary River Environments*, Lewin,
677 J., Macklin, M.G., Woodward, J.C. Eds.; Balkema: Rotterdam, The Netherlands, 1995, pp. 263-281. ISBN
678 9054101911

679 36. Kelly, M.; Black, S.; Rowan, J.S. A calcrete-based U/Th chronology for landform evolution in the Sorbas
680 basin, southeast Spain. *Quat. Sci. Rev.* **2000**, *19*, 995-1010.
681 [https://doi.org/10.1016/S0277-3791\(99\)00050-5](https://doi.org/10.1016/S0277-3791(99)00050-5)

682 37. Candy, I.; Black, S.; Sellwood, B. U-series isochron dating of immature and mature calcretes as a basis
683 for constructing Quaternary landform chronologies for the Sorbas basin, southeast Spain. *Quat. Res.*
684 **2005**, *64*, 100-111. <https://doi.org/10.1016/j.yqres.2005.05.002>

685 38. Ilott, S.H., 2013. Cosmogenic dating of fluvial terraces in the Sorbas basin, SE Spain. PhD Thesis,
686 University of Plymouth, Plymouth, 2013.

687 39. Balco, G.; Stone, J. O.H.; Lifton, N.; Dunai, T., 2008. A complete and easily accessible means of
688 calculating surface exposure ages or erosion rates from Be and Al measurements. *Quaternary*
689 *Geochronology*, *3*, 174-195.

690 40. García-Meléndez, E.; Goy, J.L.; Zazo, C. Neotectonics and Plio-Quaternary landscape development
691 within the eastern Huércal-Overa Basin (Betic Cordilleras, Southeast Spain). *Geomorphology* **2003**, *50*,
692 111–133. [https://doi.org/10.1016/S0169-555X\(02\)00210-6](https://doi.org/10.1016/S0169-555X(02)00210-6)

693 41. Stokes, M. Plio-Pleistocene drainage development in an inverted sedimentary basin: Vera basin, Betic
694 Cordillera, SE Spain. *Geomorphology* **2008**, *100*, pp.193-211.
695 <https://doi.org/10.1016/j.geomorph.2007.10.026>

696 42. Farines, B.; Calvet, M.; Gunnell, Y. The summit erosion surfaces of the inner Betic Cordillera: Their
697 value as tools for reconstructing the chronology of topographic growth in southern Spain.
698 *Geomorphology* **2015**, 233, pp.92-111. <https://doi.org/10.1016/j.geomorph.2014.11.019>

699 43. Centro Nacional de Información Geográfica. Centro de Escargas. Available online
700 <http://centrodedescargas.cnig.es/CentRodescargas/> (accessed 14/06/2018)

701 44. Boulton, S.J.; Stokes, M. Which DEM is best for analyzing fluvial landscape development in
702 mountainous terrains? *Geomorphology* **2018**, 310, pp.168-187.
703 <https://doi.org/10.1016/j.geomorph.2018.03.002>

704 45. ESRI, How To: Identify ridgelines from a DEM. Available online
705 <https://support.esri.com/en/technical-article/000011289> (accessed 14/06/2018)

706 46. Alexander, R.W.; Calvo-Cases, A.; Arnaud-Rosalén, E.; Mather, A.E., Lázaro-Suau, R. Erosion and
707 stabilisation sequences in relation to base level changes in the El Cautivo badlands, SE Spain.
708 *Geomorphology* **2008**, 100, pp.83-90. <https://doi.org/10.1016/j.geomorph.2007.10.025>

709 47. Della Seta, M.; Del Monte, M.; Fredi, P.; Miccadei, E.; Nesci, O.; Pambianchi, G.; Piacentini, T.; Troiani,
710 F. Morphotectonic evolution of the Adriatic piedmont of the Apennines: an advancement in the
711 knowledge of the Marche-Abruzzo border area. *Geomorphology* **2008**, 102, pp.119-129.
712 <https://doi.org/10.1016/j.geomorph.2007.06.018>

713 48. Pérez-Peña, J.V.; Azañón, J.M.; Azor, A.; Tuccimei, P.; Della Seta, M.; Soligo, M. Quaternary landscape
714 evolution and erosion rates for an intramontane Neogene basin (Guadix-Baza basin, SE Spain).
715 *Geomorphology* **2009**, 106 pp.206-218. <https://doi.org/10.1016/j.geomorph.2008.10.018>

716 49. Antón, L.; Muñoz-Martín, A.; De Vicente, G. Quantifying the erosional impact of a continental-scale
717 drainage capture in the Duero Basin, northwest Iberia. *Quat. Res.* **2018**, pp.1-15.
718 <https://doi.org/10.1017/qua.2018.38>

719 50. Geach, M.R.; Stokes, M.; Telfer, M.W.; Mather, A.E.; Fyfe, R.M.; Lewin, S. The application of geospatial
720 interpolation methods in the reconstruction of Quaternary landform records. *Geomorphology* **2014**, 216,
721 234-246. <https://doi.org/10.1016/j.geomorph.2014.03.036>

722 51. Rodés, Á.; Pallàs, R.; Ortuño, M.; García-Meléndez, E.; Masana, E. Combining surface exposure dating
723 and burial dating from paired cosmogenic depth profiles. Example of El Límite alluvial fan in Huércal-
724 Overa basin (SE Iberia). *Quat. Geochron.* **2014**, 19, pp.127-134.
725 <https://doi.org/10.1016/j.quageo.2013.10.002>

726 52. Hancock, G.S.; Anderson, R.S.; Chadwick, O.A.; Finkel, R.C. Dating fluvial terraces with ^{10}Be and ^{26}Al
727 profiles: application to the Wind River, Wyoming. *Geomorphology* **1999**, 27, 41-60.
728 [https://doi.org/10.1016/S0169-555X\(98\)00089-0](https://doi.org/10.1016/S0169-555X(98)00089-0)

729 53. Braucher, R.; Merchel, S.; Borgomano, J.; Bourlès, D. Production of cosmogenic radionuclides at great
730 depth: a multi element approach. *Earth Planet. Sci. Lett.* **2011**, 309, 1-9.
731 <https://doi.org/10.1016/j.epsl.2011.06.036>

732 54. Granger, D.E.; Smith, A.L. Dating buried sediments using radioactive decay and muogenic production
733 of ^{26}Al and ^{10}Be . *Nucl. Instr. Methods Phys. Res. Section B: Beam Interactions Mater. Atoms* **2000**, 172, 822-
734 826. [https://doi.org/10.1016/S0168-583X\(00\)00087-2](https://doi.org/10.1016/S0168-583X(00)00087-2)

735 55. Granger, D.E.; Muzikar, P.F. Dating sediment burial with in situ-produced cosmogenic nuclides:
736 theory, techniques, and limitations. *Earth Planet. Sci. Lett.* **2001** 188 (1-2), 269-281.
737 [https://doi.org/10.1016/S0012-821X\(01\)00309-0](https://doi.org/10.1016/S0012-821X(01)00309-0)

738 56. Balco, G.; Rovey, C.W. An isochron method for cosmogenic-nuclide dating of buried soils and
739 sediments. *Am. J. Sci.* **2008**, 308, 1083-1114.

740 57. Balco, G.; Stone, J. O.H.; Lifton, N. and Dunai, T. A complete and easily accessible means of calculating
741 surface exposure ages or erosion rates from Be and Al measurements. *Quat. Geochron.* **2008**, 3, 174-195.
742 <https://doi.org/10.1016/j.quageo.2007.12.001>

743 58. Lal, D. Cosmic ray labelling of erosion surfaces: in situ nuclide production rates and erosion models.
744 *Earth Planet. Sci. Lett.* **1991**, 104, 424 – 439. [https://doi.org/10.1016/0012-821X\(91\)90220-C](https://doi.org/10.1016/0012-821X(91)90220-C)

745 59. CRONUS Calculator 2.3 Available online <https://hess.ess.washington.edu/> accessed 04/06/2018

746 60. Mather, A.E.; Harvey, A.M.; Stokes, M. Quantifying long-term catchment changes of alluvial fan
747 systems. *Geol. Soc. Am. Bull.* **2000**, 112, pp.1825-1833.
748 [https://doi.org/10.1130/0016-7606\(2000\)112%3C1825:QLTCCO%3E2.0.CO;2](https://doi.org/10.1130/0016-7606(2000)112%3C1825:QLTCCO%3E2.0.CO;2)

749 61. Mather, A.E.; Westhead, K. Plio/Quaternary strain of the Sorbas Basin, SE Spain: evidence from soft
750 sediment deformation structures. *Quat. Proc.* **1993**, *3*, pp. 57-65.

751 62. Nash, D.J.; Smith, R.F. Multiple calcrete profiles in the Tabernas Basin, southeast Spain: their origins
752 and geomorphic implications. *Ear. Surf. Proc. Land.* **1998**, *23*, pp.1009-1029.
753 [https://doi.org/10.1002/\(SICI\)1096-9837\(1998110\)23:11%3C1009::AID-ESP918%3E3.0.CO;2-Z](https://doi.org/10.1002/(SICI)1096-9837(1998110)23:11%3C1009::AID-ESP918%3E3.0.CO;2-Z)

754 63. King, L. The pediment landform: some current problems. *Geol. Mag.* **1949**, *86*, pp.245-250.
755 <https://doi.org/10.1017/S0016756800074665>

756 64. Dumas, B. Glacis et croutes calcaires dans le Levant espagnol. *Bull. Assoc. Géog. Fran* **1969**, *46*, pp.553-
757 561.

758 65. Strudley, M.W.; Murray, A.B. Sensitivity analysis of pediment development through numerical
759 simulation and selected geospatial query. *Geomorphology* **2007**, *88*, pp.329-351.
760 <https://doi.org/10.1016/j.geomorph.2006.12.008>

761 66. Hodge, E.J.; Richards, D.A.; Smart, P.L.; Andreo, B.; Hoffmann, D.L.; Matthey, D.P.; González-Ramón,
762 A. Effective precipitation in southern Spain (~ 266 to 46 ka) based on a speleothem stable carbon
763 isotope record. *Quat. Res.* **2008**, *69*, pp.447-457. <https://doi.org/10.1016/j.yqres.2008.02.013>

764 67. Carrión, J.S.; Fernández, S.; Jiménez-Moreno, G.; Fauquette, S.; Gil-Romera, G.; González-Sampériz, P.;
765 Finlayson, C. The historical origins of aridity and vegetation degradation in southeastern Spain. *J. Arid
766 Env.* **2010**, *74*, pp.731-736. <https://doi.org/10.1016/j.jaridenv.2008.11.014>

767 68. Martrat, B.; Jimenez-Amat, P.; Zahn, R.; Grimalt, J.O. Similarities and dissimilarities between the last
768 two deglaciations and interglaciations in the North Atlantic region. *Quat. Sci. Rev.* **2014**, *99*, pp.122-134.
769 <https://doi.org/10.1016/j.quascirev.2014.06.016>

770 69. Pla-Pueyo, S.; Viseras, C.; Soria, J.M.; Tent-Manclús, J.E.; Arribas, A. A stratigraphic framework for the
771 Pliocene–Pleistocene continental sediments of the Guadix Basin (Betic Cordillera, S. Spain). *Quat. Int.*
772 **2011**, *243*, pp.16-32. <https://doi.org/10.1016/j.quaint.2011.01.028>

773 70. Braga, J.C.; Martín, J.M.; Quesada, C. Patterns and average rates of late Neogene-Recent uplift of the
774 Betic Cordillera, SE Spain. *Geomorphology* **2003**, *50*, 3–26. [https://doi.org/10.1016/S0169-555X\(02\)00205-2](https://doi.org/10.1016/S0169-555X(02)00205-2)

775 71. Stokes, M., Mather, A.E., Belfoul, A., Farik, F. Active and passive tectonic controls for transverse
776 drainage and river gorge development in a collisional mountain belt (Dades Gorges, High Atlas
777 Mountains, Morocco). *Geomorphology* **2008**, *102*, 2-20. <https://doi.org/10.1016/j.geomorph.2007.06.015>

778 72. Harvey, A.M.; Silva, P.; Mather, A.E.; Goy, J.; Stokes, M.; Zazo, C. The impact of Quaternary sea level
779 and climatic change on coastal alluvial fans in the Cabo de Gata ranges, southeast Spain. *Geomorphology*
780 **1999**, *28*, 1–22. [https://doi.org/10.1016/S0169-555X\(98\)00100-7](https://doi.org/10.1016/S0169-555X(98)00100-7)

781 73. Pastor, A.; Babault, J.; Teixell, A.; Arboleya, M.L. Intrinsic stream-capture control of stepped fan
782 pediments in the High Atlas piedmont of Ouarzazate (Morocco). *Geomorphology* **2012**, *173*, pp.88-103.
783 <https://doi.org/10.1016/j.geomorph.2012.05.032>

784 74. Völk, H.R. Quartare Reliefentwicklung in Sudost-Spanien. Heidelberger Geographische Arbeiten,
785 Germany, 1979 143pp.

786 75. Stokes, M. Plio-Pleistocene drainage evolution of the Vera Basin, SE Spain, PhD Thesis, University of
787 Plymouth, 1997.

788 76. Stokes, M.; Mather, A.E. Response of Plio-Pleistocene alluvial systems to tectonically induced base-
789 level changes, Vera Basin, SE Spain. *J. Geol. Soc.* **2000**, *157*(2), pp.303-316.
790 <https://doi.org/10.1144/jgs.157.2.303>

791 77. Wenzens, G. Mittelquartäre klimaverhältnisse und reliefentwicklung im semiariden becken von Vera
792 (Südostspanien). *Eiszeitalter und Gegenwart* **1992**, *42*, pp.121-133.

793 78. Wenzens, G. The influence of tectonics and climate on the Villafranchian morphogenesis in semiarid
794 Southeastern Spain. *Zeits. f. Geomor* **1992**, *84*, 173-184.

795 79. Wenzens, G. Die Quartäre küstenentwicklung im mündungsbereich der flüsse Aguas, Antas und
796 Almanzora in Südostspanien. *Erd undliches Wissen*, **1991** *105*, pp. 131-150.

797 80. Meikle, C.; Stokes, M.; Maddy, D. Field mapping and GIS visualisation of Quaternary river terrace
798 landforms: an example from the Rio Almanzora, SE Spain. *Journal of Maps* **2010**, *6*, pp.531-542.
799 <https://doi.org/10.4113/jom.2010.1100>

801 81. Silva, P.G.; Roquero, E.; López-Recio, M.; Huerta, P.; Martínez-Graña, A.M. Chronology of fluvial
802 terrace sequences for large Atlantic rivers in the Iberian Peninsula (Upper Tagus and Duero drainage
803 basins, Central Spain). *Quat. Sci. Rev.* **2017**, *166*, pp.188-203.
804 <https://doi.org/10.1016/j.quascirev.2016.05.027>

805 82. Santisteban, J.I.; Schulte, L. Fluvial networks of the Iberian Peninsula: a chronological framework.
806 *Quat. Sci. Rev.* **2007**, *26*, pp.2738-2757. <https://doi.org/10.1016/j.quascirev.2006.12.019>

807 83. Antón, L.; De Vicente, G.; Muñoz-Martín, A.; Stokes, M. Using river long profiles and geomorphic
808 indices to evaluate the geomorphological signature of continental scale drainage capture, Duero basin
809 (NW Iberia). *Geomorphology* **2014**, *206*, pp.250-261. <https://doi.org/10.1016/j.geomorph.2013.09.028>

810 84. Gibbard, P.L.; Lewin, J. River incision and terrace formation in the Late Cenozoic of Europe.
811 *Tectonophysics* **2009**, *474*, pp.41-55.

812 85. Bellin, N.; Vanacker, V.; Kubik, P.W. Denudation rates and tectonic geomorphology of the Spanish
813 Betic Cordillera. *Ear. Plan. Sci. Lett.* **2014**, *390*, pp.19-30.